Cumulative Dissertation

A lean magnesium-zinc-calcium alloy ZX00 used for bone fracture stabilization in a large growing-animal model and in the first clinical implementation for medial malleolus fractures in adults

Submitted by

Dr.med.univ. Patrick Holweg

For the Academic Degree of

Doctor of Medical Science

(Dr. scient. med.)

at the

Medical University of Graz

Department of Orthaepedic and Trauma Surgery

under the supervision of

Univ. Prof. Dr. Franz Josef Seibert

2020

Statutory Declaration

I hereby declare that this thesis is my own original work and that I have fully acknowledged by name all of those individuals and organisations that have contributed to the research for this thesis. Due acknowledgement has been made in the text to all other material used. Throughout this thesis and in all related publications I followed the ”Standards of Good Scientific Practice and Ombuds Committee at the Medical University of Graz”.

Patrick Holweg

Graz, December 2020

Disclosures

This thesis has been published in the following original papers:

- Holweg, P; Berger, L; Cihova, M; Donohue, N; Clement, B; Schwarze, U; Sommer, NG; Hohenberger, G; van den Beucken, JJJP; Seibert, F; Leithner, A; Löffler, JF; Weinberg, AM; A lean magnesium-zinc-calcium alloy ZX00 used for bone fracture stabilization in a large growing-animal model. Acta Biomater. 2020; 113(10):646-659

- Holweg, P; Herber, V; Ornig, M; Hohenberger, G; Donohue, N; Puchwein, P; Leithner, A; Seibert, F; A lean bioabsorbable magnesium-zinc-calcium alloy ZX00 used for operative treatment of medial malleolus fractures: early clinical results of a prospective non-randomized first in man study. Bone Joint Res. 2020; 9(8):477-483

- Holweg,P; Dauwe,J; Grechenig, P; Holter,M; Staresinic,M; Feigl,G; Bakota,B; Screw placement in two different implants for proximal humeral fractures regarding regional differences in bone mineral density: An anatomical study; *Injury* 9 October 2020*;* PII: S0020-1383(20)30848-2

I hereby confirm, that all co-authors declare that they have no conflicts of interest with the content of this thesis and have explicitly agreed to use their data in the thesis.

Doctoral candidate Patrick Holweg was trained within the frame of the Doctoral Program of Medical Science at the Doctoral school Bone, Muscle and Joint of the Medical University of Graz.

The pilot study “A lean bioabsorbable magnesium-zinc-calcium alloy ZX00 used for operative treatment of medial malleolus fractures: early clinical results of a prospective non-randomized first in man study” was supported by the Lorenz Böhler Fond.

Production and analysis of the raw material were performed by the ETH Zurich (Laboratory of Metal Physics and Technology, Department of Materials, Vladimir-Prelog-Weg 4, 8093 Zurich, Switzerland). **Berger L., Cihova M. and Löffler JF.** contributed to the preclinical publication by describing the rationale behind the development of the resorbable implant ZX00.

Danksagung

An dieser Stelle möchte ich mich bei meiner Ehefrau Sarah Holweg für ihre großartige Unterstützung während meiner gesamten beruflichen Laufbahn und ihrem unermüdlichen Einsatz bei der Erziehung unserer Buben bedanken.
Weiters gilt mein Dank dem gesamten Studienteam um Prof. Dr. Weinberg sowie dem klinisch involvierten Kollegen Dr. Ornig.
Besonders hervorheben möchte ich auch den Support durch meine Hauptbetreuer Univ. Prof. Dr. Franz Josef Seibert, Univ- Ass.in Nicole Sommer, PhD und Univ. Prof. Dr. Obermayer- Pietsch.

Table of Contents

Zusammenfassung

Biologisch abbaubare Materialien sind zunehmend im Blickpunkt der Forschung. Diese Implantatmaterialien müssen eine gute Biokompatibilität, eine vorhersagbare Resorbierbarkeit und ausreichende mechanische Festigkeit aufweisen, um eine adäquate Frakturstabilisierung, sowie eine homogene Resorbierbarkeit zu gewährleisten.

Ziel der präklinischen Studie war es, die resorbierbare Magnesiumlegierung Mg–0.45Zn–0.45Ca, in wt.% (ZX00) erstmalig in ihrer klinischen Anwendbarkeit zu evaluieren. Die Legierung wurde in einer Großtierstudie im Schaf mit osteotomiertem Knochen (Simulation eines Bruches) eingesetzt und hinsichtlich Abbauverhalten, Wachstumsregulation und Frakturheilung mit einer Kontrollgruppe ohne Osteotomie verglichen. Anhand der gesammelten Ergebnisse konnte nach erfolgter Zulassung durch die zuständige Ethikkommission und dem Bundesministerium für Gesundheit und Ernährungssicherheit eine prospektive Studie zur Anwendung dieses neuen Magnesium(Mg)-basierten Implantates (ZX00) im Rahmen der Fixierung von Innenknöchelbrüchen beim Menschen durchgeführt werden.

In der präklinischen Studie wurde kein signifikanter Unterschied zwischen dem osteotomierten Knochen und der Kontrollgruppe hinsichtlich der Änderung des Schraubenvolumens im Nachuntersuchungszeitraum gefunden. Daraus kann geschlossen werden, dass der Frakturheilungsprozess keinen signifikanten Einfluss auf das Abbauverhalten hat. Weiterführend gab es keinen negativen Einfluss der Wasserstoffgasbildung auf die Bruchheilung. Nach 12 Wochen wurden bei allen untersuchten Tieren eine vollständige Konsolidierung der Osteotomie und keine signifikanten Unterschiede in der Länge der Tibia hinsichtlich einer Wachstumsbeeinflussung festgestellt. In der darauf anschließenden prospektiven klinischen Untersuchung der Bruchstabilisierung am Innenknöchel mit ZX00 Schrauben konnten hervorragende klinische und funktionelle Ergebnisse erzielt werden.

Abstract

Over the last decade, there has been a high demand for the development of new, alternative materials in trauma care to overcome the disadvantages associated with conventional implant materials. Magnesium (Mg)-based alloys seem to adequately address the vision of a homogeneously resorbable, biocompatible, load-bearing and functionally supportive implant. The aim of the present study was to introduce the high-strength, lean alloy Mg–0.45Zn–0.45Ca, in wt.% (ZX00), and investigate for the first time the clinical applicability of screw osteosynthesis using this alloy that is free of rare-earth elements. The alloy was deployed in a growing sheep model with osteotomized bone (simulating a fracture) and compared to a non-osteotomy control group regarding degradation behavior, growth regulation and fracture healing. Finally, a prospective, non-randomized trial for the treatment of fractures of the medial malleolus using ZX00 was conducted as a first in man study.

In vivo, no significant difference between the osteotomized bone and the control group was found regarding the change in screw volume over implantation time. It can thus be concluded that the fracture healing process, including its influencing factors on the surrounding milieu, has no significant influence on the degradation behavior. Additionally, there was no negative influence of hydrogen-gas formation on fracture healing. Despite the chronologically different releases of gas volumes between the proximal and distal screws, a complete consolidation of the osteotomy and no significant differences in tibiae length in terms of influencing the growth were found after 12 weeks for all animals investigated. Subsequently, the first prospective clinical investigation of fracture reduction and fixation using ZX00 presented excellent results concerning clinical and functional outcomes.

1 Introduction

1.1 Material for fracture stabilisation

To date, conventional, bioinert metallic implant materials such as titanium alloys or stainless steel are considered the gold standard for stabilizing bone fractures. However, the number of literature sources that critically question such conventional non-resorbable osteosynthesis materials is increasing [1,2]. Rigid internal fixation is a limitation, especially in childhood trauma. Most of these implants must be removed in a second surgery, to avoid impeding longitudinal bone growth or growth disturbances, if inserted near or in the physis [3]. These implants appear too rigid and thus exceed their purpose of stabilization and deprive the bone of its task as a load carrier. This can cause "stress shielding", which leads to reduced bone remodeling due to the implant, with subsequently higher rates of re-fractures [4-6].

Secondary operations for metal removal are not only an economic burden for the health system, but also a medical-psychological stress factor for children and their parents, with a not inconsiderable anesthetic risk. Furthermore, the biocompatibility is somewhat questionable. Wear debris of unclear toxicological or teratogenic potency can be detected, with unknown effects on the expected life span of a young person [1]. New studies show that the wear debris of material left in the body may lead to immune suppression, especially if the implanted material is of a larger size [2]. Thus, clinical evidence-based influencing factors plus socio-economic aspects and psychological components justify a new definition of an optimal osteosynthesis material for fracture stabilization.

1.2 Bioabsorbable materials for fracture stabilization

Biodegradable materials are increasingly becoming the subject of intense research [7,8] in this field. Ideal implant materials must exhibit extensive biocompatibility, predictable resorbability and sufficient mechanical strength to ensure fracture stabilization and homogeneous degradation while supporting fracture healing. Furthermore, a biodegradable material for deployment in pediatrics should not impact the physis or longitudinal growth and be resorbable without long-term complications, either locally or systemically.

Biodegradable polymers, including poly-L-lactic acid (PLLA) and poly-lactic-co-glycolic acid (PLGA), are commonly used for temporary osteosynthesis and bone grafts [9,10] as they display slow degradation rates. However, the major disadvantages of these implants are poor mechanical properties (low strength and stiffness, no weight bearing), a slow degradation rate, and acidification of the surrounding tissue caused by hydrolysis during degradation. In turn, this pH drop is suspected to cause an inflammatory response. Furthermore, the capacity of polymers to actively interact with the surrounding tissue (i.e., osteoinductivity or osteoconductivity) has not yet been demonstrated [11].

These limitations may be circumvented by biodegradable ceramics. They are promising implant material candidates, as they demonstrate high compressive strength, good biocompatibility, osteoconductivity, osseointegration and non-immunogenic properties. Ceramics used as temporary implant materials are composed of hydroxyapatite (HA), or alpha (α)- and beta (β) -tricalciumphosphates (TCP). However, these ceramics exhibit inadequately slow degradation rates (over several years) [12] and lack the required ductility and tensile strength (6-10 MPa) [13].

Among biodegradable metals, magnesium (Mg)-based implants exhibit good biocompatibility and suitable mechanical properties, with appropriate strength and ductility. These properties provide a great advantage over biodegradable polymers and ceramics and thus make Mg-based materials an appealing alternative. Several studies have demonstrated the favorable functional properties of Mg-based implants, especially their ability to support bone-fracture healing in the growing bone [14-16].

Concerns regarding these implants are related to the relatively fast degradation rate *in vivo,* which leads to substantial hydrogen-gas evolution and in turn to encapsulated gas cavities, as shown in clinical evaluations [17,18]. Recently, considerable efforts have been made to reduce the Mg-degradation rate. These efforts involve surface treatments, coatings or alloy-development strategies [19,20]. The latter approach has mainly focused on alloying rare-earth elements (REEs), such as yttrium or gadolinium, to decelerate degradation [21,22]. However, REEs were observed in *in vitro* studies to negatively affect apoptosis and the viability of immune cells [23], and in *in vivo* studies to accumulate in bones or organs [24].

1.3 Bioabsorbable magnesium (Mg) implants

At the end of the 18th century, Payr was already experimenting on magnesium plates, tubes and rods and described ideas for the application to support fracture healing [25].

Lambotte was the first in the early 20th century to use magnesium-based implants for fracture stabilization. He described the use of a plate made of pure magnesium combined with steel nails to treat a broken leg. The attempt failed due to the degeneration with massive gas formation under the skin, with consecutive removal of the implant on the 8th postoperative day. He attributed the failure to an electrochemical reaction between magnesium and steel. Consequently, together with Verbrugge, he presented the pioneering approach to being able to solve the low corrosion resistance by adding different elements [26,27,28].

In the following decades, various magnesium alloys, mainly with cadmium, aluminum or manganese, were explored and clinically tested. In the course of this work, it was proven that the implantation of magnesium alloys does not lead to an increase in magnesium concentration in the serum, nor to systemically increased inflammation values. Additionally, no inflammatory reactions were observed in the local peri-implant tissue, but on the contrary, stimulatory effects on bone healing were assessed [28,29,30].

These early approaches were therefore able to define the positive aspects of magnesium more precisely, but could not solve the negative effects of the uncontrollable tendency towards corrosion and gas formation, which lead to magnesium increasingly disappearing from the research focus on clinical application and fracture stabilization.

In 1972 Borodkin and Stroganov produced further advancements by incorporating rare earth elements into magnesium alloys (0.4–4% rare earth, 0.05–1.2% cadmium, 0.05–1.0% calcium or aluminum and variable amounts <0.8% manganese, silver, zirconium or silicide) for *in vivo* examinations. They showed a more homogeneous degradation over 5-11 months, but did not provide any information about tissue accumulation or other complications [31].

In 2005 Witte et. al investigated *in vivo* degradation in the thighs of pigs of 4 different alloys against a polymer control group (polyactide - PLA). Two alloys contained aluminum (3% in the alloy "AZ31" and 9% in "AZ91") and zinc (1% each), while the other two groups contained rare earths (4% ytrium and a total of 3% neodynium, cerium and dysprosium in "WE43" and 4% lithium, 4% aluminum and a total of 2% cerium, lanthanum, neodymium and praseodymium in "LAE442"). In microtomography with synchrotron radiation, they showed significant bone growth of the magnesium groups against the PLA control group over the course of 18 weeks. Gas formation was already evident after one week, which was released by targeted puncture and was no longer detectable after 3 weeks. The slowest corrosion rate could be shown with LAE442. The rare earths were detected in the corrosion layer by means of energy-dispersive X-ray spectroscopy, while no accumulation was found in the surrounding tissue [32].

Windhager et al. showed the first results of MgYreZr (WE43 equals) based screws for chevron osteotomy in hallux surgery in a prospective, randomized, controlled clinical pilot study in 2013. In a 6-month follow-up, he demonstrated no clinical or radiological difference between the magnesium (n = 13) and the titanium control group (n = 13) in the AOFAS (American Orthopedic Foot and Ankle Society) score, in the VAS (visual analog scale for pain) or in the ROM (range of motion). No foreign body reaction, inflammatory reactions or changes in the magnesium serum level were found [33].

In 2013 clinical study, Zhao et al. examined high-purity magnesium-based screws (n = 23) for the fixation of vascularized bone grafts with existing osteonecrosis of the femoral head. Significant satisfactory results were observed in the follow-up of 12 months in the HHP (Harris hip score) and the radiological follow-up in comparison to the control group (n = 25) without fixation [34].

Most recent reviews from 2016 to 2018 are affiliated to Pogorielov et al., Zhao et al. and Grün et al. The central point of their scientific work, the progressive development of different alloys, surface treatments, manufacturing processes, local and systemic reactions and interactions and modern *in vitro* and *in vivo* testing procedures were described. Common to all is the comparison of different alloys: Mg-aluminum, Mg-zinc, Mg with rare earths, Mg-silicon and Mg-zirconium. To date, satisfactory clinical results have mainly been described in combination with rare earths [33]. Surface treatments, thermal treatments or coatings of Mg or its alloys have tended to show longer degradation times and delayed gas formation [35,36,37].

It should be noted that despite the now clinically approved commercial distribution of Mg-based implants for fracture stabilization in adults, a lack of clarity in the data regarding the ideal alloy, a limitation of the indications due to still limited mechanical properties, and uncertainty about the long-term effects of any precipitates remains.

1.3.1 Degradation of magnesium

Pure unprotected Mg corrodes quickly in the liquid environment at neutral pH. Acidic media accelerates, whereas basic media slows down corrosion. Under physiological conditions equating to 3% sodium chloride (NaCl) solutions, 99.9% pure Mg corrodes 10.5-210 mm per year [38,39].

Exposed to the earth's atmosphere close to the ground, magnesium forms a grey oxide film of magnesium hydroxide (Mg(OH)2), which causes it to corrode more slowly. Transferred to the physiological environment, the reaction and formation of magnesium chloride and hydrogen gas occurs in the presence of chloride ions, despite the low water solubility of magnesium hydroxide. One litre of hydrogen gas is produced per gram of magnesium during complete degradation [32].

The corrosion of magnesium in the physiological environment takes place in 3 partial reaction steps [40]:

$$Mg(s) + 2H_2O \rightarrow Mg(OH)2\ (s) + H2(g)$$

$$Mg(s) + 2Cl\text{-}\ (aq) \rightarrow MgCl2$$

$$Mg(OH)2\ (s) + 2Cl\text{-} \rightarrow MgCl2$$

In 2014, Sanchez et al. summarized in a systematic review more than 100 publications regarding the *in vivo* and *in vitro* degradation of Mg and its alloys. She concluded that *in vivo* and *in vitro* results are only partially comparable due to factors that are too different, especially with regard to the timing of corrosion. As the most important parameters for *in vitro* investigations, she was able to work out the composition, temperature and pH of the solution used. *In vivo* influences are more difficult in their analysis, so no main influencing factor could be described. Regardless, the dependence on the type of organism and the associated water

content, the chloride ion content and the pH value of the environment was demonstrated [41].

In a physiological environment, such as in blood, magnesium reacts with calcium and phosphate ions, causing calcium phosphate to form the implant surface. Due to the locally high concentrations of Mg and calcium this leads to the body's own accumulation of calcium phosphate by osteoblasts and corresponding bone formation [42,43].

The most important influencing factors on the corrosion resistance of magnesium are its alloy composition, coating, surface and heat treatment [44].

Ultimately, magnesium, its alloy components and degradation products are phagocytosed by cells of the innate immune system, the macrophages. In this way, the absorbed magnesium enters the bloodstream and subsequently the storage organs, bones and muscles [45].

1.3.2 ZX00

Together with the ETH Zuerich we transitioned to lean Mg-based implant materials alloyed with only zinc (Zn) and calcium (Ca), and extensively investigated the high-strength, lean alloy Mg–1.0Zn–0.3Ca (ZX10, in wt.%) [46-49]. This alloy demonstrates suitable degradation properties, extended biocompatibility and very good mechanical properties.

In an *in vivo* study, Grün et al. [50] investigated the biological response towards ZX00 and demonstrated that the material exhibited slow and homogeneous degradation in both a growing-rat model and a growing-sheep model, with good osseointegration over an observation period of 24 weeks. No negative effects on bone remodelling or on the general growth of the animals were observed [50], demonstrating the promising performance of ZX00 for bone-implant applications.

1.4 Aim of the thesis

The major aim of the thesis was the *in vivo* investigation of screws made of ZX00 for their applicability in fracture stabilization and their degradation during bone healing in a growing animal including characterization of the near-implant environment. To analyze how the implants affect tibial growth, the implants were tested upon their implantation into a fracture site and compared with reference samples inserted at a non-fracture site.

The second aim was to evaluate the safety and performance of this material for the first time in a clinical setting. Based on these aspects, a prospective, non-randomized study was established to evaluate the clinical and functional outcomes of lean Mg compression screws composed of ZX00 in the case of fracture stabilization of the medial malleolus in humans.

2 Results

2.1 Implant degradation in a growing sheep model

In total, 44 ZX00 screws were implanted in a growing sheep model. Due to insufficient postoperative tibial segmentation, one distal left-sided screw could not be sufficiently depicted on the respective µCT scan and was therefore excluded from the analysis, resulting in a test size of 43 implants.

The mean starting volume of the proximally implanted screws was 198.4 ± 0.9 mm^3 as determined by µCT. After 3 weeks, an initial implant degradation of 8.7% to a volume of 181.21 ± 6.11 mm^3 was observed. The implant volume did not decrease between 3 and 6 weeks. After 12 weeks, approximately 9% of the implant volume had degraded to a volume of 180.68 ± 10.24 mm^3. The screw volume was significantly ($p < 0.05$) reduced for 3, 6 and 12 weeks post-surgery compared to the initial volume.

The initial volume of the implants in the tibial shaft (distal) was approximately 173.6 ± 0.2 mm^3. This decreased to 165.3 ± 3.96 mm^3 (degradation: 4.8%) after 3 weeks, increased to 166.8 ± 6.25 mm^3 (increase: 0.9%) after 6 weeks and decreased to 156.0 ± 7.20 mm^3 (degradation: 6.5%) after 12 weeks. The total degradation after 12 weeks amounted to 10.3%. A statistically significant difference ($p < 0.001$) was observed between the initial volume and the volume after 3, 6 and 12 weeks. There were no significant differences between the osteotomized side and the control side.
The initial implant surface of the proximal screws had a mean value of 359.4 ± 1.3 mm^2. This increased to 374.1 ± 26.64 mm^2 (+4.1%) after 3 weeks, decreased between 3 and 6 weeks to 364.3 ± 27.16 mm^2 (- 2.6%) and was 393.1 ± 43.64 mm^2 at 12 weeks. This represents a total surface increase of 9.4% after 12 weeks of implantation.

Concerning the distal screws, their mean surface was 319.4 ± 0.34 mm^2 at the time of implantation. It increased to 326.5 ± 14.92 mm^2 (+2.2%) after 3 weeks, to 328.4 ± 13.38 mm^2 (+ 0.6%) after 6 weeks and reached 328.8 ± 26.4 mm^2 (+ 0.1%) after 12 weeks, resulting in a total increase of 2.9%. There were no statistically significant differences between the implantation sides or groups.

In the vicinity of the proximal implants, gas cavities formed at a mean volume of 487.3 ± 367.3 mm^3 three weeks following surgery. After 6 weeks the mean gas volume accounted 284.8 ± 194.0 mm^3, and 437.2 ± 244.8 mm^3 at 12 weeks.
In the distal screws, the gas cavities had a mean volume of 226.9 ± 116.9 mm^3 after 3 weeks and increased to 270.8 ± 204.4 mm^3 (at 6 weeks) and 308.4 ± 198.1 mm^3 (at 12 weeks). There were no statistically significant differences between the implantation sides or groups.

2.2 Influence on tibial growth (LLD) in a growing sheep model

The tibial lengths were compared between the osteotomized and control sides. The length differences between the implantation sides were 1.1 mm (osteotomized: 187.6 mm, intact: 188.7 mm) after 3 weeks; 1.0 mm (osteotomized: 189.1 mm, intact: 188.2 mm) after 6 weeks; and 0.9 mm after 12 weeks (osteotomized: 193.8 mm, intact: 192.9 mm). No statistically significant differences were observed between the implantation sides or between the animal groups.

2.3 Fracture healing in a growing sheep model

Regarding fracture healing, at 3 weeks post-surgery 25% of all cases showed no consolidation, 50% an incipient and 25% a complete consolidation using the descriptive, histological assessment of the sectional fracture imaging.

The 6-weeks group had consolidated fractures in 50% of all cases and incipient consolidation in the remaining 50%. At 12 weeks, all fractures were consolidated.

2.4 Growth disturbance in a growing sheep model

Premature closing of the epiphyseal growth plate caused by crossing screws was not observed at any time. Two screws were found broken at the time of examination due to the force of growt. Both were initially set through the epiphyseal plate, unintentionally in this case. The proximal portion of the screw remained in the epiphysis, while the distal portion evidently moved away with the metaphysis as it grew.

2.5 Clinical Pilot study- ZX00 used for operative treatment of medial malleolus fractures

20 patients were enrolled into the study (11 males and 9 females with a mean age of (±SD) 40.1±14,5) between July 2018 and October 2019. The follow up time point for all patients was at least 12 weeks.
During the first screening of the patients, every patient presented with normal vital signs and ECGs were normal.

Ankle sprains caused 45% of all fractures and the rest were attributed to sports injuries (bicycle, soccer, climbing and skiing accidents). Four patients presented with traffic-related injuries (20%): 2 subjects (10%) had a bicycle accident while one had a motor bike accident and another a car accident. According to the position of the medial malleolar fracture, 13 patients had a fracture type C, 6 patients had a type B fracture, and 1 patient had a type A fracture.

2.5.1 Surgery and intra-operative outcomes

During the surgery, all Mg-based screws were fixed successfully and no intraoperative complications including screw fracture were observed. Most of the patients (60%) had an anatomic intra-operative reduction without any diastasis or gap. Thirty-five percent of the patients had a persisting gap of 1 mm and one patient had a fracture reduction with a persisting diastasis of more than 1 mm. Moreover, after surgery, one unplanned CT scan analysis, performed because of debatable reduction, showed a persisting gap of 2 mm. No patient who was included in this study required unscheduled revision.

2.5.2 Clinical and functional outcomes

After surgery, the mean visual analogue scale (VAS) was 1.6±0.6 points and 1.3±0.5 points after 2 weeks. Six weeks after surgery, all patients reported no pain (VAS 1) regarding the medial malleolus. Blood analysis and specifically the dosage of magnesium and calcium were normal at all follow up visits in the 20 patients with a magnesium concentration between 0.700 and 1.100 mmol/L and a calcium concentration between 2.20 and 2.65 mmol/L. Moreover, renal function remained stable. The difference of the total movement of the talocrural joint (dorsal flexion/plantar flexion) between the operated site and the non-operated site was 39°±12° after 2 weeks, 22°±13° after 6 weeks and decreased to 8°±11° after 12 weeks. There was a statistically significant difference between week 2 and 6 ($p \leq 0.05$) and between week 6 and week 12 ($p \leq 0.001$) concerning the difference of the total movement of the talocrural joint. At the final follow-up, the mean AOFAS score was 92.5 ±4.1 points what represents an excellent result over all patients. None of the patients showed wound healing disorders. In all patients there was no erythema, swelling, deep wound infections or implant site infections and no loosening of the implant as a result of gas evolution.

After antero-posterior and lateral X-rays analysis, the ankle fracture was healed in 18 patients (90%) after 6 weeks. After 12 weeks, all patients showed complete consolidation of the ankle fractures. Serial radiographs displayed small radiolucent zones around the screws, increasing up to week 6, with a constant period to week 12, followed by a decrease to week 24. Despite this gas formation around the screws, no encapsulation was detected. In one patient, a CT scan was performed after 52 weeks, because of uncertainty of appropriate distal tibiofibular reduction after evaluation of the radiographs. Here, a screw volume loss of about 50% was displayed. Additionally an increased endosteal bone mass at the screw head was detected.

In one patient a manifest osteoporosis was noticed before surgery. In comparison to the other patients, an increased gas formation was seen around the screws. Nevertheless, bone healing was accomplished after 6 weeks. At this time-point, a small sclerotic line could be detected at the border of the radiolucent zone to the surrounding tissue. Regardless, an increase in density in this area due to higher endosteal bone mass at the region of expressed gas at the screw could be presented at the following visits radiographs after 24 and 52 weeks.

3 Discussion

The major major aim of the present study was to investigate the clinical applicability of screw osteosynthesis using the magnesium alloy ZX00 in a growing sheep model, where osteotomized bone was compared to an intact control group regarding degradation behavior, growth regulation (leg-length differences; LLD) and fracture healing.

Concerning the implant volume, an initial rapid volume decrease of 9% within the first 3 weeks was observed for the proximal, monocortical screws close to the epiphyseal plate in the tibial plateau. Subsequently, the degradation almost stagnated up to 12 weeks *post operation*. The distal bicortical screws in the shaft area also showed an initially higher volume loss of 5% within the first 3 weeks and a further loss of 5% until 12 weeks *post operation*, giving an overall loss of 10% within 12 weeks.

The temporally different volume loss between the proximal screws surrounded with spongiose bone on all sides and the bicortically set screws in the shaft area, which pass through the medullary canal and protrude into the surrounding soft tissue at the end of the screw, can be ascribed to the presence of different tissue types surrounding the implant [51]. Mechanical forces acting on the musculature surrounding the bone-protruding implant may also add to an increased degradation rate. This phenomenon can be circumvented in the implant's clinical use in humans, in which the screw length is chosen individually to match the patient's anatomy.

Witte et al. described the generation of a direct contact between the Ca-phosphate-enriched corrosion-product layer around the implant and the surrounding tissue [32]. Any increase in volume after the initial decrease within the first 3 weeks, for both distal and proximal screws, is therefore most likely due to osseointegration of the implant and its subsequently reduced demarcation to the bone.
This phenomenon appeared especially in the first weeks before the produced gas enhanced delineation. Neither the proximal nor the distal screws showed a significant

difference between the fractured and non-fractured sides in terms of volume loss. The fracture or its healing process is therefore not expected to have an influence on the degradation behavior in terms of volume loss of the Mg screws.

The surface area of the proximal screws increased by 9.4% from the baseline until the 12th week, whereas that of the distal screws only showed an increase of 2.9%. Proximally, no difference was found between the right and left sides, while the distal screws on the left side increased in surface, especially between the 6th and 12th week, and those on the right side significantly reduced in surface during the same time interval.

The general increase in surface area between the initial situation and the 12th week, observed for both the proximal and the distal screws, indicates lateral heterogeneous corrosion attack of the implant [52]. On the other hand, the significant decrease in surface area between the 6th and 12th week on the osteotomized distal side, which correlates with a significant decrease in volume over the same time interval, may be due to an influence of the surrounding tissue, as described by Sanchez et al. [53]. In particular, the medullary canal located in the shaft area, which contains immunological cells and cytokines with corresponding chemotaxis, may influence the physiological fracture healing process, which in turn may influence the material degradation of the distal screws.

In any case, the osteotomy is accompanied by an inflammatory reaction and may thus be associated with accelerated degradation through the cofactor of the bone marrow.

However, looking at the entire set of screws, a significant difference between the fracture and the reference side could not be found, neither with respect to the overall volume loss nor with respect to the degradation of the proximal or distal parts. Therefore it must be assumed that the fracture healing process, including its influencing factors on the surrounding milieu, will not have a significant influence on the degradation behavior of ZX00 implants.

The gas volume, which forms as a consequence of Mg degradation as part of the electrochemical reaction along with the generation of magnesium hydroxide, showed a steady increase around the distal screws until the 12th week, while the gas volume around the proximal screws decreased up to the 6th week followed by an increase up to 12 weeks. A correlation between the fracture healing process and hydrogen gas volume could not be established, as there were no significant differences between the osteotomized and non-osteotomized sides. The gas formation behavior is likely to be different between the proximal screw at the cancellous bone and distal screw at the medullary canal located in the shaft area due to the influence of the peri-implant environment.

Despite the chronologically different gas volumes between the proximal and distal screws, a complete consolidation of the osteotomy and no significant difference in the tibiae length was found after 12 weeks in all animals investigated. The fracture and its impact on ZX00 degradation therefore appears to influence neither the fracture healing nor the growth potential of a growing bone. Additionally, two screws were found broken at the time of examination. This purely observation-based finding underlines the great applicability of Mg-based osteosynthesis screws for fracture stabilization in paediatric traumatology. The fracture is stabilized in the first weeks until bone healing is achieved, but the screws break when bone lengthening proceeds in the epiphyseal plate.

In current literature, one trial presents four cases of implementation of magnesium implants alloyed with REE in adolescents. Pins were used for flake fracture fixation revealing promising results [54].16 clinical trials on the clinical implementation of REE-alloyed magnesium implants have been reported in adults [55-69]. The first clinical trials focused on metatarsal osteotomy fixation for the correction of hallux valgus deformities [59]. Apart from these promising results, poor outcomes were reported in two studies with extensive gas formation, loosening and cyst formation within carpal bones after scapho-trapezio-trapezoid (STT) fusion [55] and after acute scaphoid fracture fixation [56].

From our point of view, the size of the bone and its capacity to distribute the evolving gas plays an import role. Therefore we predict a higher risk for failure in small bones, caused by accumulation of trapped gas, as illustrated in recent literature [55,56].

Lee et al. [70] tested in a single centre trial the performance of Mg-5Ca-1Zn (in wt.%) (XZ51), an Mg-Ca-Zn alloy with significantly larger Ca content and Ca-to-Zn ratio than in the alloy ZX00 used in this study in the treatment of hand fractures. A total of 53 cases with a follow up of 12 months revealed excellent results without a single failure after 6 and 12 months post-implantation. None of the patients experienced a decline in grip power and the range of motion in the wrist joint remained unchanged.

Considering clinical applicability, a crucial aspect of resorbable Mg-implants must be explained. This issue concerns the widely discussed radiolucent zones around the implant caused by gas formation. In our research we have observed increased radiolucency to a certain degree, followed by a constant period and finally, recurrent increase in density develops in this area. This probably develops due to higher endosteal bone mass at the region of gas expression around the screw over time. This observation-based finding of newly formed endosteal bone, visible as increased density in the radiolucent areas, is possibly caused by the osteoinductive effect of Mg screws, which thereby compensates for the negative impact of gas expression in early stages. If hydrogen gas evolution exceeds a certain limit, the radiolucent areas formed by trapped gas are at risk of forming encapsulated gas cavities, which are edged by a sclerotic line seen in radiographs.

In our opinion, these encapsulated gas cavities are a pre-stage to persisting osteolysis and must be avoided. We did not observe loosening of any screws and no cystic encapsulation. Based on our preclinical testing, we expect the implants to completely dissolve within two years.

There are some limitations to this study. The follow-up ended after complete consolidation of the bone was achieved after 12 weeks. No statement can be made regarding long term outcome and complete dissolving of the implants. Regarding growth disturbance and fracture consolidation, there was no control group without ZX00. Growth disturbance testing focused on the impact of the artificial fracture on ZX00, while considering possible effects on bone lengthening. Therefore, the osteotomized side was compared to the intact side (LLD). Fracture healing was evaluated via serial radiological assessment using CT scans until complete consolidation of the bone was achieved.

Based on these promising results in the growing sheep model, we decided to launch the first clinical implementation of this implant ZX00. The prospective clinical trial investigated on functional and radiological results of medial malleus fracture fixation with rare earth free magnesium screws ZX00. The encouraging results of this first in man study demonstrate an adequate fixation of medial malleolus fractures with lean magnesium bioabsorbable screws. Despite the radiolucent areas around the screws at the first 12 weeks after implantation, all fractures healed without secondary dislocation or implant breakage.

An increased gas formation was seen around the screws in one patient with a manifest osteoporosis. To our knowledge, metabolic and immunological changes due to osteoporotic disease can cause an increased degradation of magnesium implants with expanded gas volume, seen as radiolucent areas. However, further investigations should focus on this highly sensitive elderly patient collective to understand the importance and underlying mechanism of osteoporosis in combination with Mg implants. Nevertheless, in this patient bone healing was accomplished after 6 weeks. Astonishingly, an obvious increase in density at the radiolucent area within the sclerotic line was observed after 52 weeks. In our opinion, this finding of newly formed endosteal bone mass demonstrates the osteoinductive effect of the Mg screws, which prevailes over the negative impact of gas expression on the long run.

Another important fact is the possible circumvention of implant site infections by Mg-based implants. Among published literature, 16 studies have been conducted with Mg based materials (54-69) with 243 surgeries. In only 2 out of all cases, a deep wound infection was described, resulting in a very small overall infection rate of 0,82%. This finding supports our opinion regarding the anti-inflammatory property of Mg implants.

Finally, this study will be extended up to 2 years to visualize the complete degradation of the material and a full conversion of the radiolucent zones formed by expressed gas into newly formed endosteal bone mass. Additionally, measurements of long-term functional outcomes will be performed.

There are some limitations of this study. Since this is the first implementation of this lean Mg material (ZX00) in humans, a control group was ethically not allowed to be established. However, 20 patients were included in the study and visited until at least bone healing was achieved.

4 Conclusion

The first study demonstrated that reducing the Zn content of ZX10 to 0.45 wt.% (0.17 at.%) and balancing the Ca content to 0.45 wt.% (0.27 at.%) lead to a superior material termed ZX00 that shows improved mechanical strength and reduced *in vitro* degradation rate. Experiments with ZX00 screws showed that in spite of, or perhaps because of, the factors influencing screw degradation, all osteotomies showed complete consolidation after twelve weeks at most. Tibiae lengths at individual time points showed no difference between the osteotomized and non-osteotomized sides, despite osteosynthesis being performed close to the physis. In summary, ZX00 screws exhibited degradation behavior comparable with the control group, did not affect growth, and achieved complete consolidation of the osteotomy.

The following clinical investigation aimed to study the performance and safety of this new material, therefore vital parameters as well as laboratory parameters in combination with clinical outcome and radiographic monitoring were performed. It can be stated that lean bioabsorbable magnesium screw fixation for displaced medial malleolus fractures provided unimpeded fracture healing. All vital and laboratory parameters were normal and the patients presented a very good functional outcome.

5 Literature

[1] Metallosis & Metal Poisoning: Hip Replacement Complications. DrugwatchCom n.d. https://www.drugwatch.com/hip-replacement/metallosis/ (accessed December 26, 2018).

[2] P. Thomas, M. Thomas, B. Summer, K. Dietrich, M. Zauzig, E. Steinhauser, V. Krenn, H. Arnholdt, M.J. Flaig, Impaired Wound-healing, Local Eczema, and Chronic Inflammation Following Titanium Osteosynthesis in a Nickel and Cobalt-allergic Patient: A Case Report and Review of the Literature, J. Bone. Joint. Surg. Am. 93 (2011) e61.

[3] A.M. Weinberg, Tscherne Unfallchirurgie: Unfallchirurgie im Kindesalter - Teil 1: Allgemeiner Teil, Kopf, Obere Extremität - Teil 2: Untere Extremität, Wirbelsäule, Körperhöhlen, Besonderheiten des kindlichen Skelettes, Springer, Berlin/Heidelberg, 2006.

[4] J. Nagels, M. Stokdijk, P.M. Rozing, Stress shielding and bone resorption in shoulder arthroplasty, J. Shoulder. Elbow. Surg. 12 (2003) 35–39.

[5] P. Augat, U. Simon, A. Liedert, L. Claes, Mechanics and mechano-biology of fracture healing in normal and osteoporotic bone, Osteoporos. Int. J. Establ. Result. Coop. Eur. Found. Osteoporos. Natl. Osteoporos. Found. USA. 16 Suppl 2 (2005) S36-43.

[6] F. Marco, F. Milena, G. Gianluca, O. Vittoria, Peri-implant osteogenesis in health and osteoporosis, Micron. 36 (2005) 630-644.

[7] W.R. Walsh, N.J. Cotton, P. Stephens, J.E. Brunelle, A. Langdown, J. Auld, F. Vizesi, W. Bruce, Comparison of poly-L-lactide and polylactide carbonate interference screws in an ovine anterior cruciate ligament reconstruction model, Arthroscopy. 23 (2007) 757-65.

[8] U. Thormann, V. Alt, L. Heimann, C. Gasquere, C. Heiss, G. Szalay, J. Franke, R. Schnettler, K.S. Lips, The biocompatibility of degradable magnesium interference screws: an experimental study with sheep, BioMed Res. Int. 2015 (2015) 1–15. article ID 943603.

[9] T. Bizenjima, T. Takeuchi, F. Seshima, A. Saito, Effect of poly (lactide-co-glycolide) (PLGA)-coated beta-tricalcium phosphate on the healing of rat calvarial bone defects: a comparative study with pure-phase beta-tricalcium phosphate, Clin. Oral. Implants. Res. 27 (2016) 1360–1367.

[10] B. Zhao, X. Qiu, D. Wang, H. Li, X. He, Application of bioabsorbable screw fixation for anterior cervical decompression and bone grafting. Clinics. 71 (2016) 320.

[11] N.G. Grün, P.L. Holweg, N. Donohue, T. Klestil, A.M. Weinberg, Resorbable implants in pediatric fracture treatment, Innov. Surg. Sci. 3 (2018) 119–125.

[12] B. León, J. Jansen (Eds.), Thin Calcium Phosphate Coatings for Medical Implants [Internet]. New York, NY: Springer New York; 2009 [cited 2017 Oct 6]. Available from: http://link.springer.com/10.1007/978-0-387-77718-4

[13] J. Black, Biological Performance of Materials: Fundamentals of Biocompatibility, fourth ed., CRC Press, 2005.

[14] L. Wu, F. Feyerabend, A.F. Schilling, R. Willumeit-Römer, B.J.C. Luthringer, Effects of extracellular magnesium extract on the proliferation and differentiation of human osteoblasts and osteoclasts in coculture, Acta. Biomater. 27 (2015) 294–304.

[15] K. Jähn, H. Saito, H. Taipaleenmäki, A. Gasser, N. Hort, F. Feyerabend, H. Schlüter, J.M. Rueger, W. Lehmann, R. Willumeit-Römer, E. Hesse, Intramedullary Mg2Ag nails augment callus formation during fracture healing in mice, Acta. Biomater. 36 (2016) 350–360.

[16] Y. Zhang, J. Xu, Y.C. Ruan, M.K. Yu, M. O'Laughlin, H. Wise, D. Chen, L. Tian, D. Shi, J. Wang, S. Chen, J.Q. Feng, D.H. Chow, X. Xie, L. Zheng, L. Huang, S. Huang, K. Leung, N. Lu, L. Zhao, H. Li, D. Zhao, X. Guo, K. Chan, F. Witte, H.C. Chan, Y. Zheng, L. Qin, Implant-derived magnesium induces local neuronal production of CGRP to improve bone-fracture healing in rats, Nat. Med. 22 (2016) 1160-1169.

[17] M. Cheng, T. Wahafu, G.G. Jiang, W. Liu, Y.Q. Qiao, X.C. Peng, T. Cheng, X.L. Zhang, G. He, X.Y. Liu, A novel open-porous magnesium scaffold with controllable microstructures and properties for bone regeneration, Sci. Rep.

[18] P. Makkar, S.K. Sarkar, A.R. Padalhin, B.-G. Moon, Y.S. Lee, B.T. Lee, In vitro and in vivo assessment of biomedical Mg–Ca alloys for bone implant applications, J. Appl. Biomater. Funct. Mater. 16 (2018) 126–136.

[19] K. Pichler, T. Kraus, E. Martinelli, P. Sadoghi, G. Musumeci, P.J. Uggowitzer, A.M. Weinberg, Cellular reactions to biodegradable magnesium alloys on human growth plate chondrocytes and osteoblasts, Int. Orthop. 38 (2014) 881-889.

[20] A. Myrissa, S. Bräuer, E. Martinelli, R. Willumeit-Römer, W. Gössler, A.M. Weinberg, Gadolinium accumulation in organs of Sprague–Dawley® rats after implantation of a biodegradable magnesium-gadolinium alloy, Acta. Biomater. 48 (2017) 521–529.

[21] A. Myrissa, A. Nezha Ahmad, Y. Lu, E. Martinelli, J. Eichler, G. Szakacs, C. Kleinhans, R. Willumeit-Römer, U. Schäfer, A.M. Weinberg, In vitro and in vivo comparison of binary Mg alloys and pure Mg, Mater. Sci. Eng. C. Mater. Biol. Appl. 61 (2016) 865–874.

[22] F. Amerstorfer, S. Fischerauer, L. Fischer, J. Eichler, J. Draxler, A. Zitek, M. Meischel, E. Martinelli, T. Kraus, S. Hann, S.E. Stanzl-Tschegg, P.J. Uggowitzer, J.F. Löffler, A.M. Weinberg, T. Prohaska, Long-term in vivo degradation behavior and near-

implant distribution of resorbed elements for magnesium alloys WZ21 and ZX50, Acta. Biomater. 42 (2016) 440–450.

[23] L. Jin, J. Wu, G. Yuan, T. Chen, In vitro study of the inflammatory cells response to biodegradable Mg-based alloy extract, PLoS. One. 13 (2018) e0193276.

[24] S. Hirano, K.T. Suzuki, Exposure, Metabolism, and Toxicity of Rare Earths and Related Compounds, Environ. Health. Perspect. 104 Suppl 1 (1996) 85-95.

[25] E. Payr, Zur Verwendung des Magnesiums für resorbierbare Darmknöpfe und andere chirurgisch-technische Zwecke. Cent Chir 1901;28:513–5.

[26] M. Staiger, A. Pietak, J. Huadmai, G. Dias. Magnesium and its alloys as orthopedic biomaterials: A review. Biomaterials 2006;27:1728–34. doi:10.1016/j.biomaterials.2005.10.003.

[27] A. Lambotte. L'utilisation du mangesium comme meteriel perdu sans l'osteosynthèse. vol. 28, Bull Mém Soc Nat Chir; 1932, p. 1325–34.

[28] J. Verbrugge. L'utilisation du magnésium dans le traitement chir- urgical des fractures [The use of magnesium in the surgical treat- ment of fractures]. Bull Mém Soc Nat Cir 1937;59:813–23.

[29] E. McBRIDE. ABSORBABLE METAL IN BONE SURGERY: A FURTHER REPORT ON THE USE OF MAGNESIUM ALLOYS. J Am Med Assoc 1938;111:2464–7. doi:10.1001/jama.1938.02790530018007.

[30] V. Troitskii, D. Tsitrin. The resorbing metallic alloy 'Osteosinthezit' as material for fastening broken bone. Khirurgiia (Sofiia) 1944;8:41–4.

[31] G. Stroganov, E. Savitsky, T. Mikhailovich, M. Nina, V. Terekhova, V. Fedorovna, et al. Magnesium-base alloys for use in bone surgery. US Patent No. 3687135A 1972.

[32] F. Witte. In vivo corrosion of four magnesium alloys and the associated bone response. Biomaterials 2005;26:3557–63. doi:10.1016/j.biomaterials.2004.09.049.

[33] H. Windhagen, K. Radtke, A. Weizbauer, J. Diekmann, Y. Noll, U. Kreimeyer, et al. Biodegradable magnesium-based screw clinically equivalent to titanium screw in hallux valgus surgery: short term results of the first prospective, randomized, controlled clinical pilot study. Biomed Eng Online 2013;12:62. doi:10.1186/1475-925X-12-62.

[34] D.Zhao, S. Huang, F. Lu, B. Wang, L.Yang , L. Qin, et al. Vascularized bone grafting fixed by biodegradable magnesium screw for treating osteonecrosis of the femoral head. Biomaterials 2016;81:84–92. doi:10.1016/j.biomaterials.2015.11.038.

[35] N. Grün, N. Donohue, P. Holweg, A. Weinberg. Resorbierbare Implantate in der Unfallchirurgie. J Für Miner Muskuloskelettale Erkrank 2018;25:82–9. doi:10.1007/s41970-018-0041-6.

[36] M. Pogorielov, E. Husak, A. Solodivnik, S. Zhdanov. Magnesium-based biodegradable alloys: Degradation, application, and alloying elements. Interv Med Appl Sci 2017;9:27–38. doi:10.1556/1646.9.2017.1.04

[37] D. Zhao, F. Witte, F. Lu, J. Wang, J. Li, L. Qin. Current status on clinical applications of magnesium-based orthopaedic implants: A review from clinical translational perspective. Biomaterials 2017;112:287–302. doi:10.1016/j.biomaterials.2016.10.017.

[38] H. Inoue, K. Sugahara, A. Yamamoto, H. Tsubakino. Corrosion rate of magnesium and its alloys in buffered chloride solutions. Corros Sci 2002;44:603–10. doi:10.1016/S0010-938X(01)00092-0.

[39] P. Miller, B. Shaw, R. Wendt, W. Moshier. Assessing the Corrosion Resistance of Nonequilibrium Magnesium-Yttrium Alloys. CORROSION 1995;51:922–31. doi:10.5006/1.3293568.

[40] B. Shaw. Corrosion resistance of magnesium alloys. vol. 13A. ASM International; 2003.

[41] A. Sanchez, B. Luthringer, F. Feyerabend, R. Willumeit . Mg and Mg alloys: How comparable are in vitro and in vivo corrosion rates? A review. Acta Biomater 2015;13:16–31. doi:10.1016/j.actbio.2014.11.048.

[42] E. Zhang, L. Xu, G. Yu, F. Pan, K. Yang. In vivo evaluation of biodegradable magnesium alloy bone implant in the first 6 months implantation. J Biomed Mater Res A 2009;90:882–93. doi:10.1002/jbm.a.32132.

[43] L. Xu, G. Yu, E. Zhang, F. Pan, K. Yang. In vivo corrosion behavior of Mg-Mn-Zn alloy for bone implant application. J Biomed Mater Res A 2007;83:703–11. doi:10.1002/jbm.a.31273.

[44] J. Gray, B. Luan. Protective coatings on magnesium and its alloys — a critical review. J Alloys Compd 2002;336:88–113. doi:10.1016/S0925-8388(01)01899-0.
64
[45] N. Saris, E. Mervaala, H. Karppanen, J. Khawaja, A. Lewenstam. Magnesium. An update on physiological, clinical and analytical aspects. Clin Chim Acta Int J Clin Chem 2000;294:1–26.

[46] J. Hofstetter, M. Becker, E. Martinelli, A.M. Weinberg, B. Mingler, H. Kilian, S. Pogatscher, P.J. Uggowitzer, J.F. Löffler, High-strength low-alloy (HSLA) Mg–Zn–Ca alloys with excellent biodegradation performance, JOM. 66 (2014) 566–572.

[47] J. Hofstetter, S. Ruedi, I. Baumgartner, H. Kilian, B. Mingler, E. Povoden-Karadeniz, S. Pogatscher, P.J. Uggowitzer, J.F. Löffler, Processing and microstructure–property relations of high-strength low-alloy (HSLA) Mg–Zn–Ca alloys, Acta. Mater. 98 (2015) 423–432.

[48] S. Jafari, R. K. S. Raman, C. H. J. Davies, J. Hofstetter, P. J. Uggowitzer, J. F. Löffler, Stress corrosion cracking and corrosion fatigue characterisation of MgZn1Ca0.3 (ZX10) in a simulated physiological environment, J. Mech. Behav. Biomed. Mater. 65 (2017) 634-643.

[49] M. Cihova, E. Martinelli, P. Schmutz, A. Myrissa, R. Schäublin, A.M. Weinberg, P.J. Uggowitzer, J.F. Löffler, The role of zinc in the biocorrosion behavior of resorbable Mg–Zn–Ca alloys, Acta. Biomater. 100 (2019) 398-414.

[50] N.G. Grün, P. Holweg, S. Tangl, J. Eichler, L. Berger, J.J.J.P. van den Beucken, J.F. Löffler, T. Klestil, A.M. Weinberg, Comparison of a resorbable magnesium implant in small and large growing-animal models, Acta. Biomater. 78 (2018) 378–86.

[51] C. Rössig, N. Angrisani, P. Helmecke, S. Besdo, J. M. Seitz, B. Welke, N. Fedchenko, H. Kock, J. Reifenrath, In vivo evaluation of a magnesium-based degradable intramedullary nailing system in a sheep model, Acta Biomater. 25 (2015) 369–383.

[52] S.F. Fischerauer, T. Kraus, X. Wu, S. Tangl, E. Sorantin, A.C. Hänzi, J.F. Löffler, P.J. Uggowitzer, A.M. Weinberg, In vivo degradation performance of micro-arc-oxidized magnesium implants: a micro-CT study in rats. Acta Biomater. 9 (2013) 5411-5420.

[53] A.H.M. Sanchez, B.J.C. Luthringer, F. Feyerabend, R. Willumeit, Mg and Mg alloys: How comparable are in vitro and in vivo corrosion rates? A review. Acta Biomater. 13 (2015) 16–31.

[54] M. Rupprecht, M. Kertai, Ersten Ergebnisse mit magnesiumbasierten Implantaten im Kindes- und Jugendalter. Jatros Orthopädie & Traumatologie Rheumatolgie 2/2019

[55] A: Wichelhaus, J. Emmerich, T. Mittlmeier, A Case of Implant Failure in Partial Wrist Fusion Applying Magnesium-Based Headless Bone Screws. Case Rep Orthop. (2016) 7049130.

[56] R. Meier, M. Panzica, First results with a resorbable MgYREZr compression screw in unstable scaphoid fractures show extensive bone cysts. Handchir Mikrochir Plast Chir. 49 (2017) 37-41.

[57] R. Biber, J. Pauser, M. Geßlein, H.J. Bail, Magnesium-Based Absorbable Metal Screws for Intra-Articular Fracture Fixation. Case Rep Orthop. (2016) 9673174.

[58] Turan A, Kati YA, Acar B, Kose O. Magnesium Bioabsorbable Screw Fixation of Radial Styloid Fractures: Case Report. J Wrist Surg. 9 (2020) 150-155.

[58] C. Plaass, C. von Falck, S. Ettinger, L. Sonnow, F. Calderone, A. Weizbauer, J. Reifenrath, L. Claassen, H. Waizy, K. Daniilidis, C. Stukenborg-Colsman, H. Windhagen, Bioabsorbable magnesium versus standard titanium compression screws for fixation of distal metatarsal osteotomies - 3 year results of a randomized clinical trial. J Orthop Sci. 23 (2018) 321-327.

[60] C. Plaass, S. Ettinger, L. Sonnow, S. Koenneker, Y. Noll, A. Weizbauer, J. Reifenrath, L. Claassen, K. Daniilidis, C. Stukenborg-Colsman, H. Windhagen, Early results using a biodegradable magnesium screw for modified chevron osteotomies. J Orthop Res. 34 (2016) 2207-2214.

[61] H. Leonhardt, A. Franke, N.M.H. McLeod, G. Lauer, A. Nowak, Fixation of fractures of the condylar head of the mandible with a new magnesium-alloy biodegradable cannulated headless bone screw. Br J Oral Maxillofac Surg. 55 (2017) 623-625.

[62] R. Biber, J. Pauser, M. Brem, H.J. Bail, Bioabsorbable metal screws in traumatology: A promising innovation. Trauma Case Rep. 8 (2017) 11-15.

[63] O. Kose, A. Turan, M. Unal, B. Acar, F. Guler F, Fixation of medial malleolar fractures with magnesium bioabsorbable headless compression screws: short-term clinical and radiological outcomes in eleven patients. Arch Orthop Trauma Surg. 138 (2018) 1069-1075.

[64] B. Acar, O. Kose, A. Turan, M. Unal, Y.A. Kati, F. Guler, Comparison of Bioabsorbable Magnesium versus Titanium Screw Fixation for Modified Distal Chevron Osteotomy in Hallux Valgus. Biomed Res Int. 19 (2018) 5242806.

[65] J.T. Choo, S.H.S. Lai, C.Q.Y. Tang, G. Thevendran. Magnesium-based bioabsorbable screw fixation for hallux valgus surgery - A suitable alternative to metallic implants. Foot Ankle Surg. S1268-7731 (2018) 30392-8.

[66] H. Klauser, Internal fixation of three-dimensional distal metatarsal I osteotomies in the treatment of hallux valgus deformities using biodegradable magnesium screws in comparison to titanium screws. Foot Ankle Surg. S1268-7731 (2018) 30030-4.

[67] A. Gigante, N. Setaro, M. Rotini, S.S. Finzi, M. Marinelli, Intercondylar eminence fracture treated by resorbable magnesium screws osteosynthesis: A case series. Injury. 49 Suppl 3 (2018) S48-S53.

[68] B. Acar, M. Unal, A. Turan, O. Kose, Isolated Lateral Malleolar Fracture Treated with a Bioabsorbable Magnesium Compression Screw. Cureus. 10 (2018) e2539.

[69] C. Aktan, M.B. Ertan, A. Turan, O. Kose, Fixation of Small Osteochondral Fragments in a Comminuted Distal Humerus Fracture with Magnesium Bioabsorbable Screws: A Case Report. Cureus. 10 (2018) e3752.

[70] J.W. Lee, H.S. Han, K.J. Han, J. Park, H. Jeon, M.R. Ok, H.K. Seok, J.P. Ahn, K.E. Lee, D.H. Lee, S.J. Yang, S.Y. Cho, P.R. Cha, H. Kwon, T.H. Nam, J.H. Han, H.J. Rho, K.S. Lee, Y.C. Kim, D. Mantovani, Long-term clinical study and multiscale analysis of in vivo biodegradation mechanism of Mg alloy. Proc Natl Acad Sci U S A. 113 (2016) 716-21.

Acta Biomaterialia 113 (2020) 646–659

Contents lists available at ScienceDirect

Acta Biomaterialia

journal homepage: www.elsevier.com/locate/actbio

Full length article

A lean magnesium–zinc–calcium alloy ZX00 used for bone fracture stabilization in a large growing-animal model

Patrick Holweg[a], Leopold Berger[b], Martina Cihova[b], Nicholas Donohue[a], Bernhard Clement[a], Uwe Schwarze[a,c], Nicole G. Sommer[a], Gloria Hohenberger[a], Jeroen J.J.P. van den Beucken[d], Franz Seibert[a], Andreas Leithner[a], Jörg F. Löffler[b], Annelie-Martina Weinberg[a,*]

[a] Department of Orthopaedics and Trauma, Medical University of Graz, Auenbruggerplatz 5, 8036 Graz, Austria
[b] Laboratory of Metal Physics and Technology, Department of Materials, ETH Zurich, Vladimir-Prelog-Weg 4, 8093 Zurich, Switzerland
[c] Division of Oral Surgery and Orthodontics, Department of Dental Medicine and Oral Health, Medical University of Graz, Auenbruggerplatz 12, 8036 Graz, Austria
[d] Department of Biomaterials (309), Radboud University Nijmegen Medical Center, Philips van Leijdenlaan 25, 6525 Nijmegen, The Netherlands

ARTICLE INFO

Article history:
Received 2 March 2020
Revised 4 June 2020
Accepted 9 June 2020
Available online 14 June 2020

Keywords:
Magnesium-based implants
Growing skeleton
Fracture fixation
Degradation
Pediatric orthopedics

ABSTRACT

Over the last decade, demand has increased for developing new, alternative materials in pediatric trauma care to overcome the disadvantages associated with conventional implant materials. Magnesium (Mg)-based alloys seem to adequately fulfill the vision of a homogeneously resorbable, biocompatible, load-bearing and functionally supportive implant. The aim of the present study is to introduce the high-strength, lean alloy Mg–0.45Zn–0.45Ca, in wt% (ZX00), and for the first time investigate the clinical applicability of screw osteosynthesis using this alloy that contains no rare-earth elements. The alloy was applied in a growing sheep model with osteotomized bone (simulating a fracture) and compared to a non-osteotomy control group regarding degradation behavior and fracture healing. The alloy exhibits an ultimate tensile strength of 285.7 ± 3.1 MPa, an elongation at fracture of 18.2 ± 2.1%, and a reduced *in vitro* degradation rate compared to alloys containing higher amounts of Zn. *In vivo*, no significant difference between the osteotomized bone and the control group was found regarding the change in screw volume over implantation time. Therefore, it can be concluded that the fracture healing process, including its effects on the surrounding area, has no significant influence on degradation behavior. There was also no negative influence from hydrogen-gas formation on fracture healing. Despite the proximal and distal screws showing chronologically different gas release, the osteotomy showed complete consolidation.

Statement of Significance

Conventional implants involve several disadvantages in pediatric trauma care. Magnesium-based alloys seem to overcome these issues as discussed in the recent literature. This study evaluates the clinical applicability of high-strength lean Mg–0.45Zn–0.45Ca (ZX00) screws in a growing-sheep model. Two groups, one including a simulated fracture and one group without fracture, underwent implantation of the alloy and were compared to each other. No significant difference regarding screw volume was observed between the groups. There was no negative influence of hydrogen-gas formation on fracture healing and a complete fracture consolidation was found after 12 weeks for all animals investigated.

* Corresponding author.
E-mail address: anneliemartina.weinberg@medunigraz.at (A.-M. Weinberg).

https://doi.org/10.1016/j.actbio.2020.06.013

1. Introduction

Osteosynthesis has become the procedure of choice for unstable and displaced bones in fracture treatment in the field of pediatric orthopedics. Physicians carefully operate on immature patients after trauma to ensure appropriate longitudinal bone growth, since the vulnerable physis is responsible for longitudinal lengthening of immature bones as a result of endochondral ossification [1]. The main focus in this field is to avoid any changes by products or residues of the degradation process or any damage to the physis resulting from complications during the entire surgical treatment.

To date, conventional, bioinert metallic implant materials such as titanium alloys or stainless steel are considered the gold standard for stabilizing bone fractures in youths. However, the number of literature sources that critically question such conventional non-resorbable osteosynthesis materials is increasing [2,3]. Rigid internal fixation is a limitation, especially in childhood trauma. Most of these implants must be removed in a second surgery, to avoid impeding longitudinal bone growth or growth disturbances, if inserted near or in the physis [4]. These implants appear to be too rigid and thus exceed their purpose of stabilization and deprive the bone of its task as a load carrier. This can cause "stress shielding", which leads to reduced bone remodeling due to the implant, with subsequently higher rates of re-fractures [5–7].

Secondary operations for metal removal are not only an economic burden for the health system, but also a medical-psychological stress factor for the children and their parents, with a considerable anesthetic risk. Furthermore, the biocompatibility is somewhat questionable. Wear debris of unclear toxicological or teratogenic potency can be detected, with unknown effects on the expected life span of a young person [2]. New studies show that the wear debris of material left in the body may lead to immune suppression, especially if the implanted material is of larger size [3]. Thus, clinical evidence-based influencing factors plus socio-economic aspects and psychological components justify a new definition of an optimal osteosynthesis material for fracture stabilization.

In particular, biodegradable materials are increasingly becoming the subject of intense research [8,9] in this field. Ideal implant materials must exhibit extended biocompatibility, predictable resorbability and sufficient mechanical strength to ensure fracture stabilization and homogeneous degradation while supporting fracture healing. Furthermore, a biodegradable material for deployment in pediatrics should not impact the physis or longitudinal growth and be resorbable without long-term complications locally or systemically.

Biodegradable polymers, including poly-L-lactic acid (PLLA) and poly-lactic-co-glycolic acid (PLGA), are commonly used for temporary osteosynthesis and bone grafts [10,11] as they display slow degradation rates. However, the major disadvantages of these implants are poor mechanical properties (low strength and stiffness, no weight bearing), a slow degradation rate, and acidification of the surrounding tissue caused by hydrolysis during degradation. In turn, this pH drop is suspected to cause an inflammatory response. Furthermore, the capacity of polymers to actively interact with the surrounding tissue (i.e., osteoinductivity or osteoconductivity) has not yet been demonstrated [12].

These limitations may be circumvented by biodegradable ceramics. They are promising implant material candidates, as they demonstrate high compressive strength, good biocompatibility, osteoconductivity, osseointegration and non-immunogenic properties. Ceramics used as temporary implant materials are composed of hydroxyapatite (HA), or alpha (α)- and beta (β)-tricalciumphosphates (TCP). However, these ceramics exhibit inadequately slow degradation rates (over several years) [13] and lack the required ductility and tensile strength (6-10 MPa) [14].

Among biodegradable metals, magnesium (Mg)-based implants exhibit good biocompatibility and suitable mechanical properties, with appropriate strength and ductility. These properties provide a great advantage over biodegradable polymers and ceramics and thus make Mg-based materials an appealing alternative. Several studies have demonstrated the favorable functional properties of Mg-based implants, especially their ability to support bone-fracture healing in the growing bone [15–17].

Concerns regarding these implants are related to the relatively fast degradation rate *in vivo,* which leads to substantial hydrogen-gas evolution and in turn to encapsulated gas cavities, as shown in clinical evaluations [18,19]. Recently, considerable efforts have been made to reduce the Mg-degradation rate. These efforts involve surface treatments, coatings or alloy-development strategies [20,21]. The latter mainly focused on the alloying of rare-earth elements (REEs), such as yttrium or gadolinium, to decelerate degradation [22,23]. However, REEs were observed in *in vitro* studies to negatively affect apoptosis and the viability of immune cells [24], and in *in vivo* studies to accumulate in bones or organs [25].

In pediatric orthopedic trauma treatment it is of utmost importance to avoid both short-term and, especially, long-term adverse effects. Hence, we transitioned to lean Mg-based implant materials alloyed with only zinc (Zn) and calcium (Ca), and extensively investigated the high-strength, lean alloy Mg–1.0Zn–0.3Ca (ZX10, in wt%) [26–29]. This alloy demonstrates suitable degradation properties, extended biocompatibility and very good mechanical properties. Despite the low alloying content, ZX10 reaches a tensile yield strength of 240 MPa, an ultimate tensile strength of 270 MPa and an elongation at fracture of up to 30% [27,28] when produced via a closely controlled process comprising a sequence of heat treatments and hot extrusion [27]. In fact, these favourable mechanical properties result from controlled precipitation of nanometric intermetallic particles (IMPs), which pin the grain boundaries during hot forming and thus ensure a fine-grained microstructure [27]. In these alloys, the amount of Zn requires special attention as it is the most electropositive element in this alloying system. Zn can strongly influence degradation kinetics by governing the phase type of IMPs depending on its nominal alloying content, its content relative to Ca, and the processing conditions [29]. In direct comparison with alloys of higher Zn content (ZX50 and ZX20 with 5.0 wt% and 1.5 wt% Zn, respectively), ZX10 was found to exhibit a significantly slower degradation rate *in vitro* and *in vivo* [26,29]. Furthermore, it was recently observed that solute Zn redeposits on the dissolving Mg substrate, which leads to accelerated alloy dissolution [29]. A further reduction in Zn below the nominal content contained in ZX10 thus appears to be a promising approach to further reduce the degradation rate. However, a first attempt using Mg–0.5Zn–0.15Ca (in wt%), i.e. a material in which the alloying content is reduced by half compared to ZX10, and applying the same processing protocol as for ZX10, did not result in the desired mechanical properties [27]. The cause was the absence of IMPs, and consequently a missing grain-boundary pinning effect, resulting in a significantly larger grain size and with that in reduced grain-boundary strengthening [27].

It was hypothesized that simultaneous reduction of the Zn content and balancing of the Ca content would lead to the formation of the required IMPs at feasible extrusion temperatures, resulting in the development of ZX00 with the composition Mg–0.45Zn–0.45Ca (in wt%). In an *in vivo* study, Grün et al. [30] investigated the biological response towards ZX00 and demonstrated that the material exhibits slow and homogeneous degradation in both a growing-rat model and a growing-sheep model, with good osseointegration over an observation period of 24 weeks. No negative effects on bone remodelling or on the general growth of the animals were observed [30], demonstrating the promising performance of ZX00 for bone-implant applications. However, an inves-

tigation of the materials' mechanical performance and underlying microstructure is still required and no information on the ability of fracture stabilisation and load-bearing efficiency is available. To make these materials suitable for deployment in osteosynthesis for children, adequate stability during fracture healing [31] must be guaranteed.

The present study contains some rationale behind the development of ZX00 and presents its *in vitro* characterization. Furthermore, we investigated screws made of ZX00 *in vivo* for their applicability in fracture stabilization and their degradation during bone healing in a growing animal (including characterization of the near-implant environment). To analyze how the fracture affects implants, we tested them upon their implantation into a fracture site and compared them with reference to samples inserted at a non-fracture site.

2. Materials & methods

2.1. Material production and analysis

The alloy design of ZX00 was guided by thermodynamic calculations of possible phases in the ZX system, using the Pandat™ software package for multicomponent systems, Pandat_2019 [42], with input taken from the MatCalc database mc_mg_v1.009 [43]. The calculations assume thermodynamic equilibrium.

Ultra-high pure Mg (99.999%) [32] was alloyed with Zn (99.9999%) and Ca (99.95%) at 750°C under a protective gas atmosphere in a nominal composition of 0.45 wt% Zn and 0.45 wt% Ca. Following homogenization (350°C/ 12 h, 450°C/ 8 h; subsequent cooling with pressurized air to 200°C) and aging (250°C/ 30 min), indirect extrusion was performed at 345°C into rods of 6 mm diameter, corresponding to an extrusion ratio of 1:69. All further material characterizations were performed on the extruded rods. The alloy composition was determined by inductively coupled plasma optical emission spectrometry (ICP-OES) and trace elements were quantified by glow discharge mass spectrometry (GDMS), which entails a relative error of 20% (instrument uncertainty).

Light micrographs were prepared by mechanical grinding and polishing followed by etching with picric acid, to reveal the grain boundaries, and used for the determination of the non-recrystallized volume fraction deploying ImageJ software. In light micrographs, non-recrystallized regions can be distinguished from those of recrystallized grains due to their brighter contrast. In a first step, micrographs from cross sections perpendicular to the extrusion direction were manually optimized (brightness and contrast) for subsequent thresholding. The parameters were carefully adjusted as to provide the best possible visual correspondence with the original micrograph. The fraction of white pixels then provides the fraction of non-recrystallized regions.

The average grain size and texture characteristics were determined by electron backscatter diffraction (EBSD) on an FEI Quanta 200F with an EDAX Hikari camera and at a tilt angle of 70° and a step size of 65 nm. Specimens for EBSD analysis were prepared by mechanical grinding and polishing (diamond paste with particle size down to 0.25 µm and ultimately colloidal silica suspension with particle size of about 20 nm to minimize surface deformation). Final polishing was performed by broad ion beam milling using Ar+ ions (BIB IM4000 Hitachi; process settings: flat ion milling, 1.5 reciprocation/min, ±60-degree swing angle). Acceleration voltage was gradually decreased from 4 kV (5 min) to 3 kV (15 min) to 2 kV (45 min).

The detailed microstructure was analyzed by transmission electron microscopy (TEM) on an FEI Talos™ F200X operated at 80 kV. TEM samples were prepared as standard 3 mm disks by mechanically grinding to a thickness of about 80 µm, followed by Ar^+-ion milling (PIPS™ II from Gatan, Inc.) to achieve electron transparency. Ion milling was performed at a 3.5 ° incident angle and an acceleration voltage of 4 kV, and at liquid-nitrogen temperature to avoid changes to the microstructure. Imaging was performed in scanning-TEM (STEM) mode using a high-angle annular dark field (HAADF) detector and in TEM mode using a bright-field (BF) detector. Chemical information was obtained in STEM mode using an energy-dispersive X-ray spectroscopy (EDS) detector (FEI Super-X).

Tensile tests according to ISO 6892-1 (testing diameter: 4 mm, gauge length: 20 mm, strain rate: 8×10^{-4} s^{-1}) were performed to determine tensile yield strength (*TYS*), ultimate tensile strength (*UTS*) and elongation at fracture (*A*).

Table 1
Salts for the preparation of the simulated body fluid used in this study in the order of mixing.

Reagent	Concentration (mg l^{-1})
KCl	298.2
NaCl	5844
$NaHCO_3$	2268.5
$MgSO_4 \bullet 7H_2O$	246.5
$CaCl_2$	367.5
KH_2PO_4	136.1

2.2. Implant fabrication

Screws were manufactured using polycrystalline diamond tools without lubrication to avoid potential contamination and corrosive attack. The screws were cleaned in an ultrasonic bath in acetone, air dried in a clean-room atmosphere and sterilized by gamma irradiation (dose: 29.2 kGy).

The proximal screws were manufactured with an outer diameter of 3.5 mm and a length of 29 mm. Their initial volume was 198.4 mm^3, with a surface area of 359.8 mm^2. The screws inserted into the tibial shaft had a diameter of 3.5 mm, a length of 24 mm, a volume of 173.6 mm^3 and a surface area of 319.4 mm^2.

2.3. In vitro *degradation*

The *in vitro* degradation rate of ZX00 was evaluated by the hydrogen-gas evolution method [33], which is based on the quantification of evolving hydrogen gas as a measure for the dissolving Mg metal according to $Mg + 2H_2O \rightarrow Mg^{2+} + H_2 + 2OH^-$.

Three samples, each with a surface area of about 4.7 cm^2, were prepared by mechanical grinding of the surface with SiC4000 paper. Isopropanol (IPA) was used as a lubricant to avoid corrosive attack. Following subsequent ultrasonic cleaning in IPA, the samples were stored in IPA until shortly before the immersion to minimize oxidation.

Simulated body fluid (for the composition see Table 1) was used as an electrolyte. The temperature was kept at 37°C and the pH value was monitored and adjusted online to a stable value of 7.4 ± 0.05 by flushing the SBF with pure CO_2. An immersion setup specifically designed for the hydrogen-gas-evolution analysis of slowly degrading materials [34] was deployed. The ZX10 alloy processed according to Hofstetter et al. [26] was used as a reference. The values reported are corrected for atmospheric-pressure fluctuations and gas-solubility variations.

2.4. Ethical statement

The animal trial (Permit Number: BMWFW-66.010/0073-WF/V/3b/2015) was approved by the Austrian Federal Ministry for Science and Research and followed the guidelines on accommodation and care of animals formulated by the European Convention for the Protection of Vertebrate Animals Used for Experimental and Other Scientific Purposes.

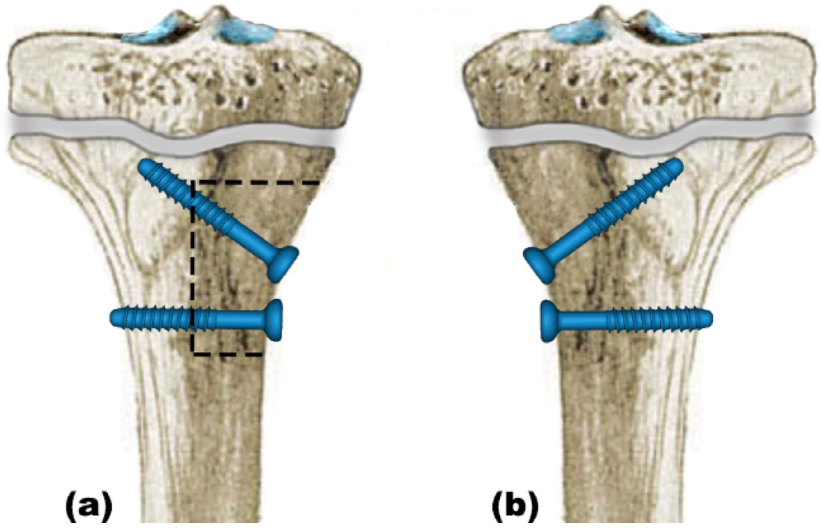

Fig. 1. Schematic depiction of (a) right-sided tibial osteotomy (black dotted line), epiphyseal plate (grey split) and ZX00 screws and (b) left tibial osteosynthesis with ZX00 screws, but without osteotomy.

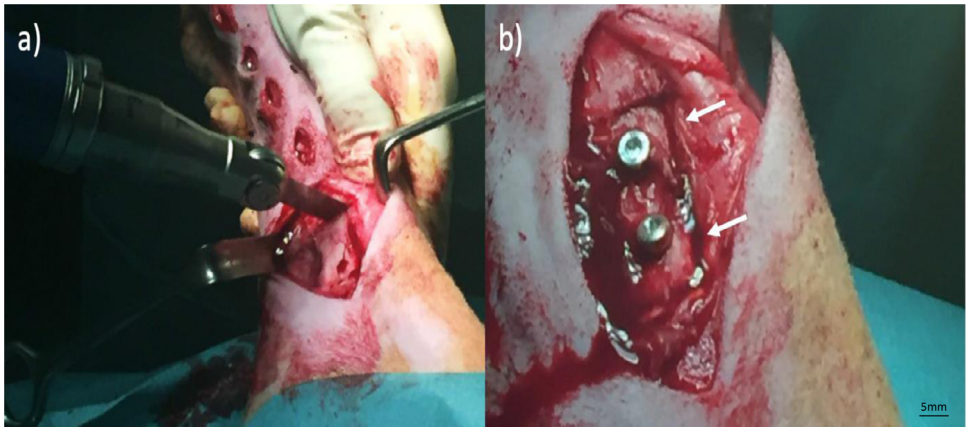

Fig. 2. (a) Surgical site with oscillating saw for osteotomy. (b) Surgical site after osteotomy and screw osteosynthesis. Arrows indicate the osteotomy.

2.5. Surgery and postoperative treatment

A total of eleven one-month-old lambs were divided into three groups with regard to the respective observation period of 3 (n=4), 6 (n=4) and 12 weeks (n=3). Each animal received pre-operative tetanus prophylaxis.

The surgical treatment principle involved an osteotomy (representing an artificial fracture) of the right tibia and refixation of the fracture with two ZX00 screws. In the left leg (control group) two ZX00 screws were inserted without an osteotomy. In both groups, the proximal screw was inserted into the proximal tibia, adjacent to or crossing the epiphyseal plate, and the distal screw was applied bicortically in the proximal tibial shaft (see Fig. 1). Whether the epiphyseal plate was crossed or not could not be verified at the time of surgery.

Surgeries were performed under sterile conditions and general anesthesia. The epiphyseal plate was located through use of intraoperative fluoroscopy. An approximately 10 cm long skin incision was performed at the proximal right-side tibia, followed by precise epiperiosteal dissection to the bone under protection of the local neurovascular bundle. The right-side osteotomy was performed using an oscillating saw with two parallel incisions and two connecting longitudinal incisions. To check the completeness of the osteotomy, the cortical fragment was raised by a few millimeters, with a subsequent reduction and screw fixation of the fragment (see Fig. 2a). Drilling was performed with a 2.7 mm drill bit and a 3.5 mm thread tapper. The proximal, monocortical screw was inserted in a latero-cranial direction into the proximal tibia and the distal, bicortical screw was applied in a strictly lateral direction to the tibial shaft (see Fig. 2b). ZX00 screw implantations in the left tibiae (control group) were performed using stab incisions. The screw positions were checked by the use of an intraoperative image converter and the tissues were closed in layers.

Postoperative analgesia involved 4 mg/kg bw carprofen (every twenty-four hours) and 0.01 mg/kg bw buprenorphine (4-times daily subcutaneous application) for four days post-surgery. Additionally, the animals received 4 mg/kg bw gentamicin and 30,000 IE/kg bw penicillin for a period of five days as postoperative infection prophylaxis. Daily wound checks were also performed.

Termination criteria involved all types of wound healing deficits, pain aggravation including inappetence and emaciation as well as tympanities.

The animals were euthanized 3, 6 and 12 weeks after surgery. Their tibiae were harvested, wrapped in saline-soaked gauze and frozen at -20°C.

2.6. Imaging and radiological analysis

The explanted tibiae underwent X-ray imaging as well as low-magnification (51.75 µm voxel size with binning setting 2) µCT

Fig. 3. X-ray imaging performed 3, 6 and 12 weeks following surgery of the right osteotomized leg and the left intact leg. Inserted screws are displayed on both sides (indicated by arrows). The fracture line in the right leg cannot be depicted in the X-ray image.

scans (µCT Siemens Inveon; Siemens Healthcare Diagnostics GmbH, Vienna, Austria) at all timepoints (3 weeks, 6 weeks, and 12 weeks). Fig. 3 gives a radiological overview for the various timepoints.

Three-dimensional post processing, segmentation and measurement of the µCT data sets were performed with MIMICS® software (version 21.0; Materialise, Leuven, Belgium). Screw degradation, size of the gas cavities and fracture healing were evaluated. The osteotomized right leg was compared to the left leg control group to evaluate the degradation behavior as a consequence of screw implantation in a fracture situation.

To evaluate fracture healing, the osteotomy (fracture) gap was assessed on the CT-scans in three planes by three independent evaluators. To classify fracture healing, three grades were utilized (see Table 2). Examples of CT-images for these three grades are shown in Fig. 4. Apart from the radiological evaluation of the frac-

Table 2
Grading of fracture consolidation including respective definition and reference to sample images.

Classification	Definition	Figure
No consolidation	The fracture gap is visible in all three planes; fracture margins have sharp limitations.	4a
Incipient consolidation	The fracture gap shows incipient consolidation including bone bridges in all three planes; fracture margins have indistinct limitations.	4b
Consolidation	The fracture gap shows bone consolidation in all three planes; fracture margins are not determinable.	4c

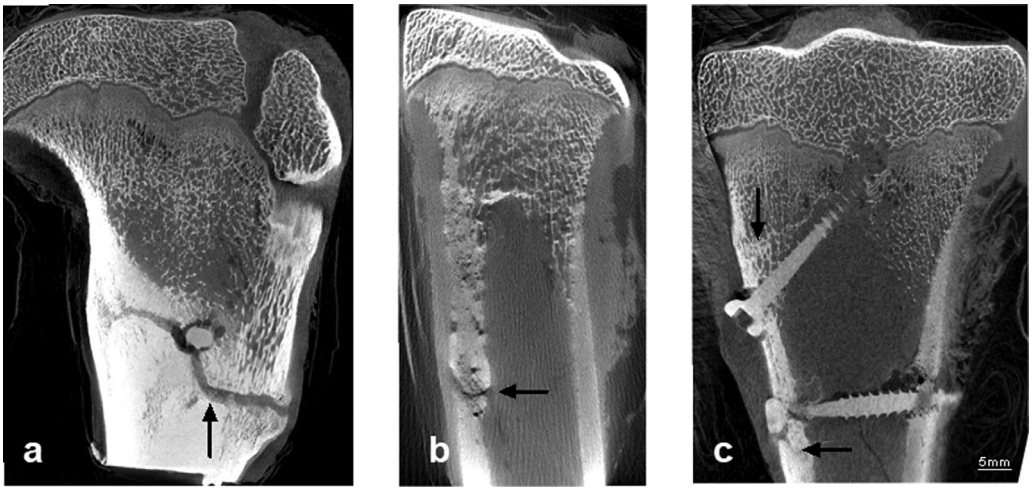

Fig. 4. Fracture healing including classification. (a) Lateral view of the proximal tibia; no consolidation: black arrow marks fracture gap. (b) Lateral view of the proximal tibia; incipient consolidation: black arrow. (c) Anterior-posterior view of the proximal tibia; consolidation: black arrow.

ture healing, we used a descriptive, histological assessment of the sectional fracture images (see Table 2).

2.7. Histological examination

The formaldehyde-fixed specimens were rinsed in water, dehydrated in ascending ethanol solutions, and then infiltrated and embedded in methylmethacrylate. The embedded blocks were serially sliced into 80 µm-thick sections using a Leica SP-1600 saw microtome. Slices were glued on glass slides and stained with a Methylene Blue and Basic Fuchsine combination and covered with a cover slip.

Qualitative histological assessment was performed to evaluate screw degradation, gas formation, soft-tissue changes and new bone formation.

2.8. Statistics

Quantitative data are reported in the form of "mean ± standard deviation". For statistical evaluation and graphic depiction, the Prism software (version 7.0a; GraphPad Software Inc., SanDiego, USA) was used. The data of the three groups (3, 6 and 12 weeks) were compared with a one-way ANOVA and the single groups were compared to each other using Tukey's multiple comparison test. To compare the intact and osteotomized sides, an Independent Samples t-Test was performed. A p-value < 0.05 was considered statistically significant.

3. Results

The effective composition of the extruded material was determined at 0.404 ± 0.008 wt% for Ca and 0.413 ± 0.007 wt% for Zn. The main trace elements are listed in Table 3.

Fig. 5 shows a simulation of the expected phases in ZX00 and their volume fraction with respect to temperature in thermodynamic equilibrium. The earlier reported alloy ZX10 [26] is additionally shown in this graph as a reference. These simulations reveal the rationale behind the chosen alloy composition. In fact, they illustrate that for ZX00 processed at 345°C a microstructure is expected that contains an intermetallic phase composed of the binary Mg_2Ca Laves phase, equivalent to that contained in ZX10. This

Table 3
Trace elements found in the extruded material as determined by glow discharge mass spectroscopy. Only elements with concentrations above 1 ppm wt. are listed.

Element	Al	Si	Fe	Ni	Pb
Concentration in ppm wt.	3.6	3.1	1.3	1.6	4.2

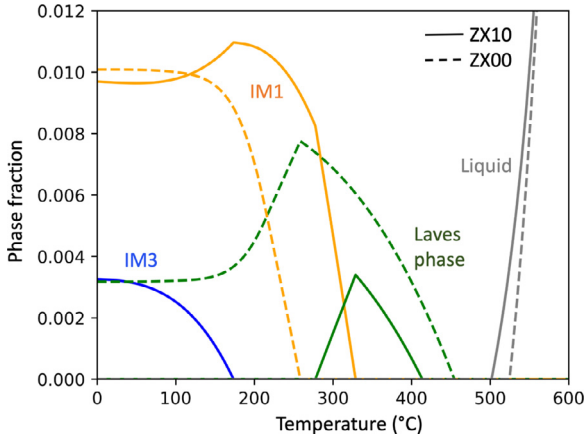

Fig. 5. Thermodynamic calculations used for alloy design. The phase fractions in thermodynamic equilibrium of the intermetallic phases Mg_2Ca (Laves phase), IM1 ($Ca_3Mg_xZn_{15-x}$ with $4.6 \leq x \leq 12$), IM3 ($Ca_xMg_yZn_z$ with $8.2 \leq x \leq 9.1$; $27.1 \leq y \leq 31.0$; $60.8 \leq z \leq 64$) [44], and the liquid phase are computed and plotted with respect to temperature for ZX00 and ZX10.

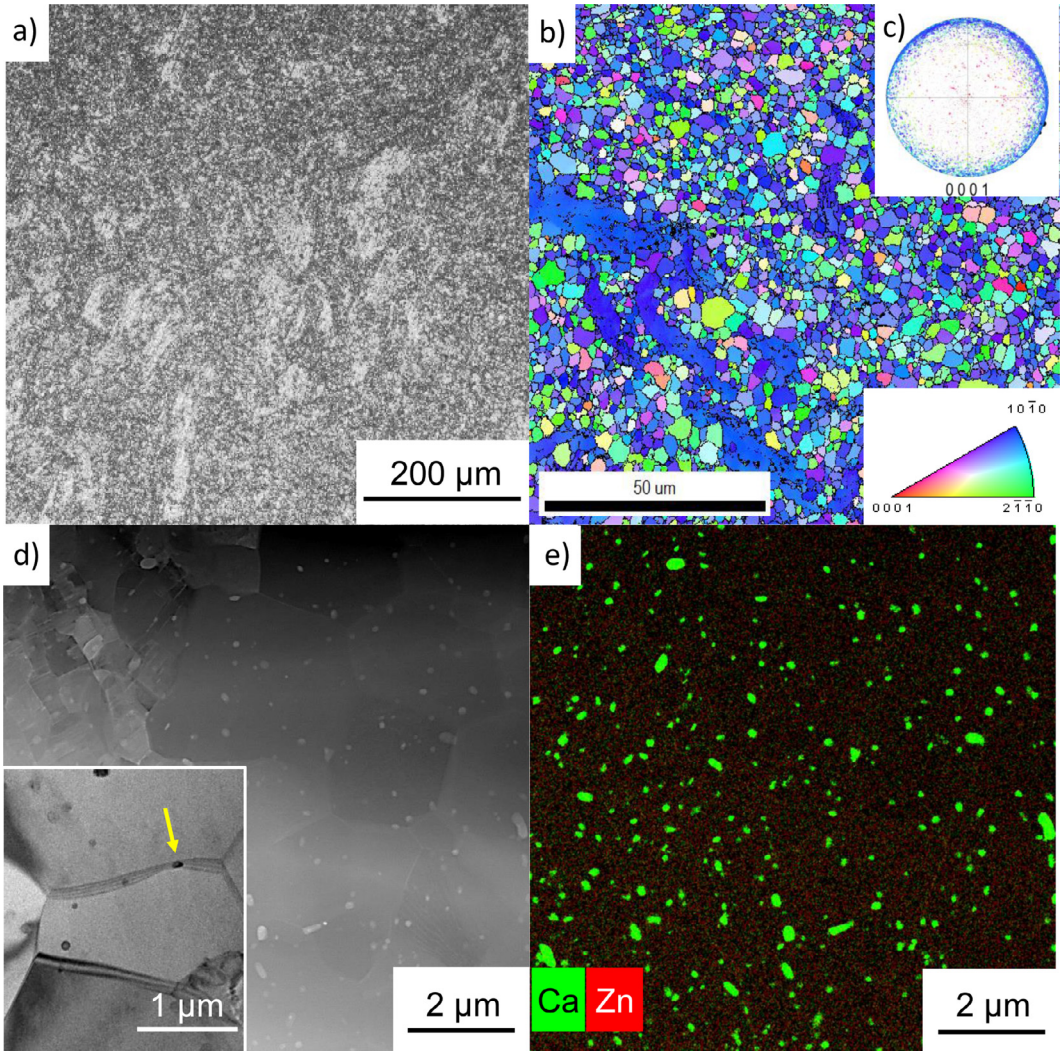

Fig. 6. Microstructure of ZX00 alloy. (a) Light micrograph and (b, c) EBSD scans obtained perpendicular to the extrusion direction, revealing (a, b) the degree of recrystallization and (b) the grain morphology and size. (c) Pole figure showing a basal texture after hot extrusion. (d, e) TEM-based analysis. (d) STEM HAADF contrast revealing the intermetallic particles in bright contrast; inset to (d) TEM bright-field image showing an IMP pinning a grain boundary (yellow arrow). (e) STEM EDS chemical map for Ca and Zn, corresponding to the area in (d), revealing that the IMPs are Ca-rich.

phase was previously reported to be beneficial for a slow degradation rate of ZX-lean alloys [26,29]. A significantly larger volume fraction of this phase is predicted in the case of ZX00. Assuming that coarse precipitation of the intermetallic phase can be avoided, its larger volume fraction is expected to generate a stronger grain-boundary pinning effect during hot extrusion, which would lead to a smaller grain size and thus higher strength of the resulting implant material.

3.1. Microstructure and mechanical properties

Fig. 6 shows the microstructure characteristic of the prepared ZX00 alloy. Low-magnification analysis based on light microscopy (Fig. 6a) reveals significantly brighter areas, which account for about 20% of the surface area and presumably correspond to a non-recrystallized microstructure. Electron backscatter diffraction (Fig. 6b, c) exhibits a bimodal grain-size distribution and texturized microstructure. Roughly equiaxed grains in the recrystallized regions with an average size of 1.67 ± 0.84 µm are interspersed with clearly larger, non-recrystallized regions. Furthermore, a pronounced basal texture is observed with the basal planes oriented preferentially parallel to the extrusion direction (Fig. 6c).

High-resolution analysis based on TEM (Fig. 6d,e) reveals the presence of nanometric IMPs, which are visible in bright contrast in STEM-HAADF mode (Fig. 6d), indicative for their enrichment in higher-atomic number (Z) elements. The IMPs were found within the matrix grains and along the grain boundaries. Those present at grain boundaries were occasionally observed to interact with the grain boundaries, causing their bowing (inset to Fig. 6d). This observation shows the important role of IMPs in grain-size control by effective grain-boundary pinning. Chemical analysis using EDS (Fig. 6e) reveals that the IMPs are composed of a phase rich in Mg and Ca, visible from the green contrast image, with green assigned to Ca. Note that Mg is not shown in the chemical map of Fig. 6e for the sake of legibility. Zn, in contrast, appears roughly homogeneously distributed within the Mg matrix and the IMPs.

Notably, the microstructure contained some areas with significantly smaller grains (Fig. 6d, top left). The IMPs' characteristics in these areas, however, appeared consistent with those of larger-grain areas in terms of morphology, size or chemical composition. Highly deformed, non-recrystallized regions were not observed in the TEM foil.

Tensile tests revealed a pronounced yield-point phenomenon with an average tensile yield strength of 283.6 ± 5.0 MPa and an average ultimate tensile strength of 285.7 ± 3.1 MPa for ZX00.

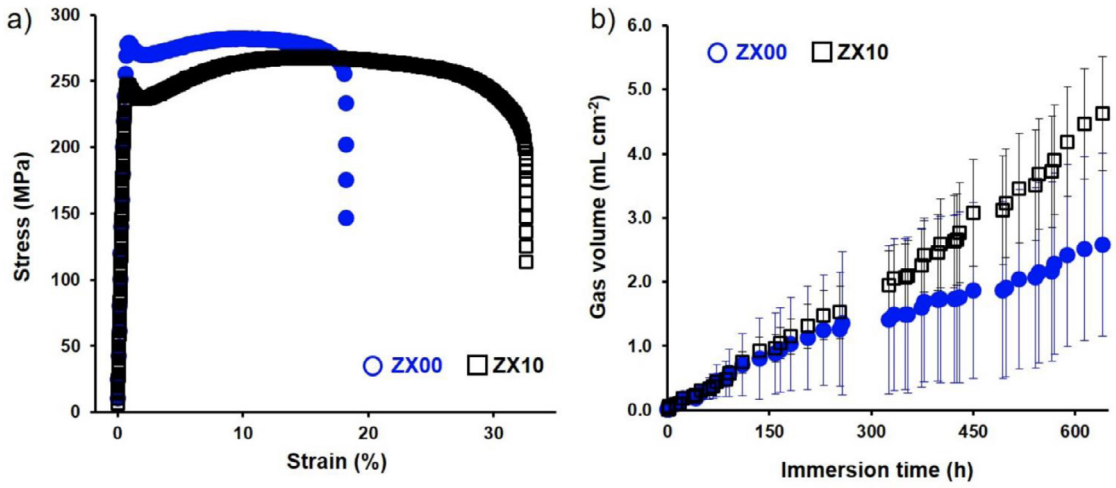

Fig. 7. (a) Stress-strain curves of as-extruded ZX00 and ZX10. The stress-strain curve for ZX10 is obtained from Ref. [28]. (b) Gas-volume evolution upon immersion in SBF over an immersion time of 4 weeks for ZX00 and ZX10.

The average elongation at fracture was determined at 18.2 ± 2.1%. Fig. 7 shows a characteristic stress-strain curve for ZX00 in comparison to ZX10.

3.2. In vitro *degradation*

Fig. 7b shows the gas volume evolving for ZX00 and ZX10 upon their immersion in SBF over the course of 4 weeks. Initially, approximately for the first five days the released gas volume was roughly the same for both materials. For the subsequent immersion, the gas volume evolving from ZX10 was slightly larger compared to that of ZX00 and the difference in evolving gas volume appeared to increase with longer immersion time. However, the difference was not statistically significant at any time.

3.3. In vivo *implant degradation*

In total, 44 ZX00 screws were implanted. Due to insufficient postoperative tibial segmentation, one distal left-sided screw could not be sufficiently depicted on the respective µCT scan and was therefore excluded from the analysis, resulting in a test size of 43 implants.

The mean starting volume of the proximally implanted screws was 198.4 ± 0.9 mm^3 as determined by µCT. After 3 weeks, an initial implant degradation of 8.7% to a volume of 181.2 ± 6.1 mm^3 was observed. The implant volume did not decrease between 3 and 6 weeks. After 12 weeks, approximately 9% of the original implant volume had degraded to a volume of 180.7 ± 10.2 mm^3. The screw volume was significantly ($p < 0.05$) reduced for 3, 6 and 12 weeks post-surgery compared to the initial volume (see Fig. 8).

The initial volume of the implants in the tibial shaft (distal) was approximately 173.6 ± 0.2 mm^3. This decreased to 165.3 ± 4.0 mm^3 (degradation: 4.8%) after 3 weeks, increased to 166.8 ± 6.3 mm^3 (increase: 0.9%) after 6 weeks and decreased to 156.0 ± 7.2 mm^3 (degradation: 6.5%) after 12 weeks (see Fig. 8). The overall degradation after 12 weeks amounted to 10.1%. A statistically significant difference ($p < 0.001$) was observed between the initial volume and the volumes after 3, 6 and 12 weeks. There were no significant differences between the osteotomized side and the control side.

The initial implant surface of the proximal screws had a mean value of 359.4 ± 1.3 mm^2. This increased to 374.1 ± 26.6 mm^2 (+4.1%) after 3 weeks, decreased between 3 and 6 weeks to 364.3 ± 27.2 mm^2 (-2.6%) and increased to 393.1 ± 43.6 mm^2 at 12 weeks (+7.9%) (see Fig. 9). This represents a total surface increase of 9.4% after 12 weeks of implantation. Concerning the distal screws, their mean surface was 319.4 ± 0.3 mm^2 at the time of implantation. It increased to 326.5 ± 14.9 mm^2 (+2.2%) after 3 weeks, to 328.4 ± 13.4 mm^2 (+ 0.6%) after 6 weeks and reached 328.8 ± 26.4 mm^2 (+ 0.1%) after 12 weeks, resulting in a total increase of 2.9%. There were no statistically significant differences between the implantation sides or groups (see Fig. 9).

3.4. *Gas formation*

In the vicinity of the proximal implants, gas cavities formed at a mean volume of 487.3 ± 367.3 mm^3 three weeks following surgery. After 6 weeks the mean gas volume amounted to 284.8 ± 194.0 mm^3, and after 12 weeks to 437.2 ± 244.8 mm^3 (see Fig. 10).

In the distal screws, the gas cavities had a mean volume of 226.9 ± 116.9 mm^3 after 3 weeks (see Fig. 10 and 3D model in Fig. 11) and increased to 270.8 ± 204.4 mm^3 (at 6 weeks) and 308.4 ± 198.1 mm^3 (at 12 weeks). There were no statistically significant differences between the implantation sides or groups.

3.5. *Fracture healing*

Regarding fracture healing, at 3 weeks post-surgery 25% of all cases showed no consolidation, 50% an incipient and 25% a complete consolidation using the descriptive, histological assessment of the sectional fracture imaging (see Table 2 and Fig. 4).

The 6-weeks group had consolidated fractures in 50% of all cases and incipient consolidation in the remaining 50%. At 12 weeks, all fractures were consolidated.

3.6. *Growth disturbance*

Premature closing of the epiphyseal growth plate caused by crossing screws was not observed at any time. Two screws were found broken at the time of examination due to the force of growth (see Figs. 12 and 13). Both were initially set through the epiphyseal plate, unintentionally in this case. The proximal portion of the screw remained in the epiphysis, while the distal portion evidently moved away due to the growth of the metaphysis (see Figs. 12 and 13).

3.7. *Descriptive histological evaluation*

Fig. 14 shows histological slices stained with a Methylene Blue and Basic Fuchsine combination for the control and fracture groups

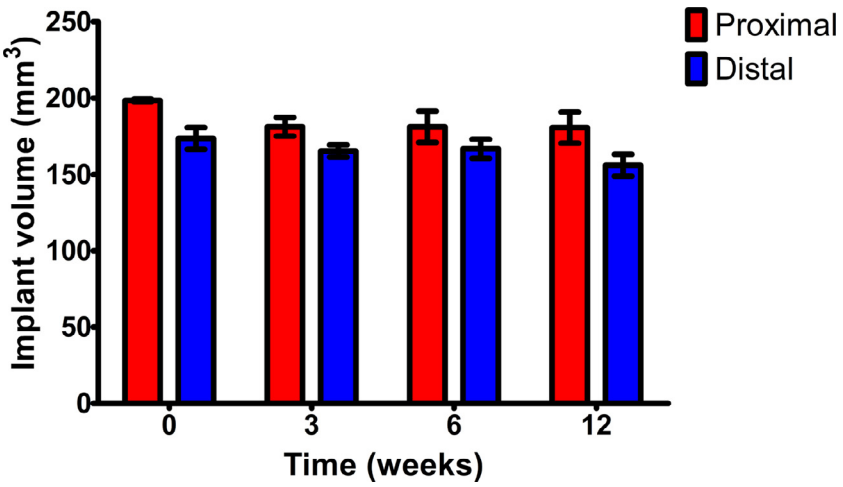

Fig. 8. Implant volume of the entire proximal and distal screws presented as mean ± standard deviation.

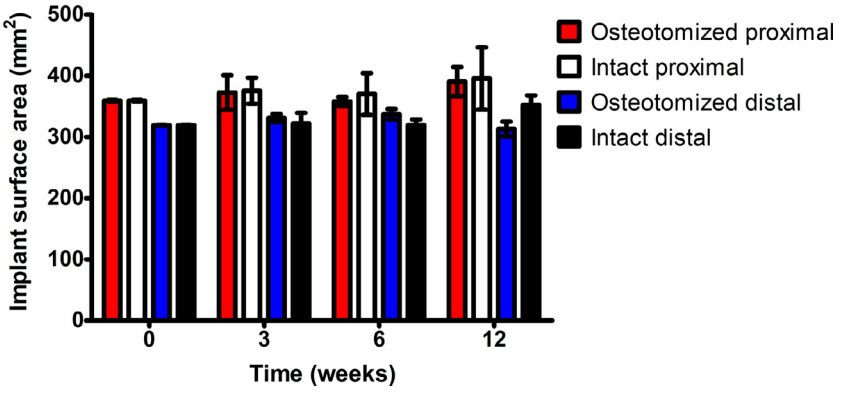

Fig. 9. Implant surface of the proximal and distal screws of the osteotomized and intact side presented as mean ± standard deviation.

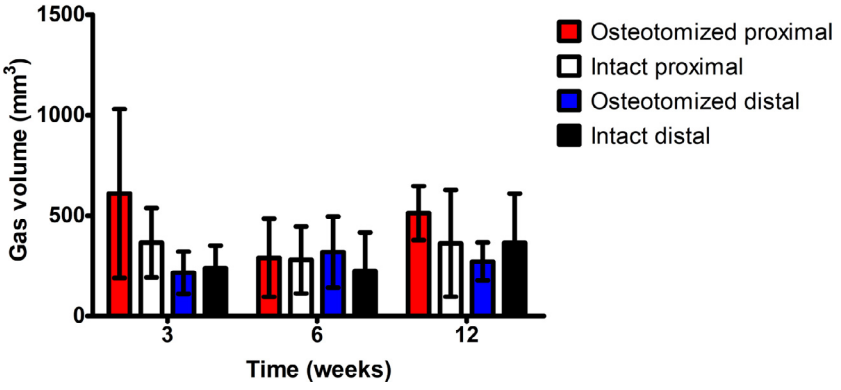

Fig. 10. Gas volume of the proximal and distal screws of the osteotomized and intact side presented as mean ± standard deviation.

after 12 weeks of implantation. The dyes stain soft tissue blue and calcified tissue in shades of pink, with older bone appearing lighter than younger bone. The histological evaluation revealed homogeneous and occasionally lacuna-shaped degradation of the ZX00 screws. The screws were still preserved to a large extent after 12 weeks, and the shaft, head and threads are still easily discernible (see Fig. 14), with corrosion products surrounding the metallic screw and reaching a layer thickness of approximately 150 µm. The corrosion products are stained pink, similar to bone. This is not surprising considering the corrosion products *in vivo* to be rich in Ca and P and thus chemically similar to bone [35]. Distinguishable characteristics between the corrosion products and bone are the shade, morphology, and the existence of osteocytes [35,36].

The screws were surrounded by gas cavities with flattened and compressed soft tissue on their border. However, no fibrous capsules were observed. Developing bone near the growth plate appeared to be slightly more mature in the growth-plate penetration region than in the more superficial zones of the growth plate. Bone formation in the form of tapestry-like layers of woven and parallel-fibered bone occurred on the metallic and corrosion-product screw surfaces. Direct bone-to-implant contact varied from small regions to large parts of the implant. The bone layers were up to 150 µm wide. The corrosion products were also covered by thin layers of bone with a width of about 43 µm. After 12 weeks of implantation the fracture group seemed to have slightly larger bone area around the implants than the control group. No other differences were ob-

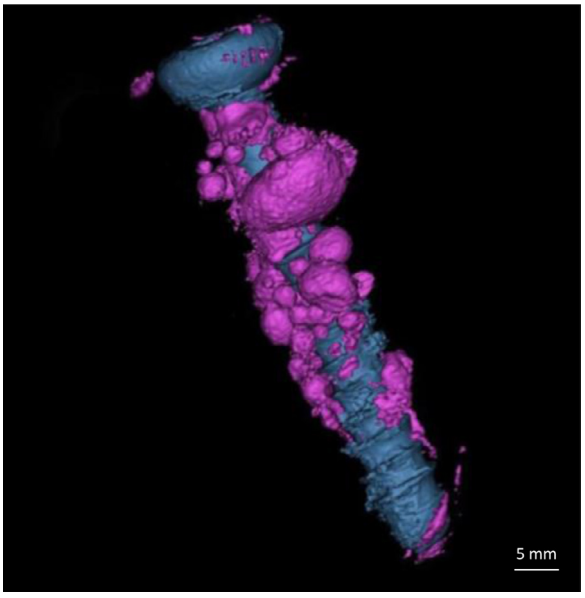

Fig. 11. 3D model of the distal screw for the osteotomized side (blue) after 3 weeks of degradation, with surrounding hydrogen gas measured as gas cavities (magenta).

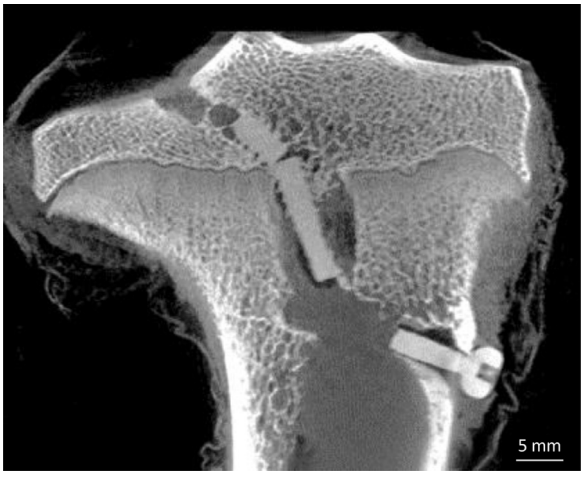

Fig. 12. Broken screw in the 12-weeks group with transepiphyseal position.

served between these groups. The bone area on the screw surface was larger after 12 weeks than after 6 weeks, and larger after 6 weeks than after 3 weeks. No other differences between the time points were recognized histologically (see Fig. 14).

4. Discussion

One objective of this study was to demonstrate the feasibility of further reducing the alloying content in biodegradable high-strength lean Mg–Zn–Ca alloys, with the intention of reducing the degradation rate while still maintaining good mechanical properties, in comparison to the well-reported ZX10 alloy. The Zn-to-Ca ratio was balanced, resulting in Mg–0.45Zn–0.45Ca, termed ZX00.

Similar to comparable alloys with slightly higher alloying content [27, 29], a mainly fine-grained microstructure was found (Fig. 6). Larger non-recrystallized regions were also present in a volume fraction of approximately 20%. Microstructural data revealed nanometer-sized intermetallic particles (IMPs), composed of a Ca-rich phase (Fig. 6e), indicating that they are composed of the Laves-type phase Mg_2Ca. The presence of this phase agrees with predictions obtained by thermodynamic calculations (Fig. 5), validating the underlying thermodynamic model and supporting the suitability to design Mg–Zn–Ca lean alloys based on such calculations. The average size of the recrystallized grains in ZX00 (1.67 ± 0.83 µm) is comparable to the values reported for ZX10 (1.6 µm to 5.1 µm) [27]. Considering grain-boundary strengthening to be the dominant strengthening mechanism of the recrystallized portion of these low-alloyed Mg–Zn–Ca alloys [27], comparable values for the *TYS* are expected, following the well-known Hall–Petch relationship [64]. In fact, the *TYS* for ZX00 was found to be even higher, with about 284 MPa for ZX00 and about 240 MPa for ZX10 (Fig. 7a). Also, the *UTS* of ZX00 at 285.7 ± 3.1 MPa was higher compared to that of ZX10 at 240-268 MPa. The increased strength concurred with a loss in ductility, with an elongation at fracture of 18.2 ± 2.1% for ZX00 compared to 20-32% for ZX10 [27] (Fig. 7a), which is explained by the higher fraction of non-recrystallized microstructure in ZX00 and the strong basal texture (Fig. 6b,c). These large non-recrystallized regions are a result of the extrusion process, which imposes severe plastic deformation on the original microstructure, and with that leads to a strong increase in dislocation density. The high number of dislocations hinders the movement of any other dislocations, thereby increasing the material's strength [65]. The elongation at fracture, although reduced compared to ZX10, was found to outperform that of many other magnesium alloys, most notably the above mentioned clinically proven extruded XZ51 alloy (A = 9%) [62]. This can be explained by the

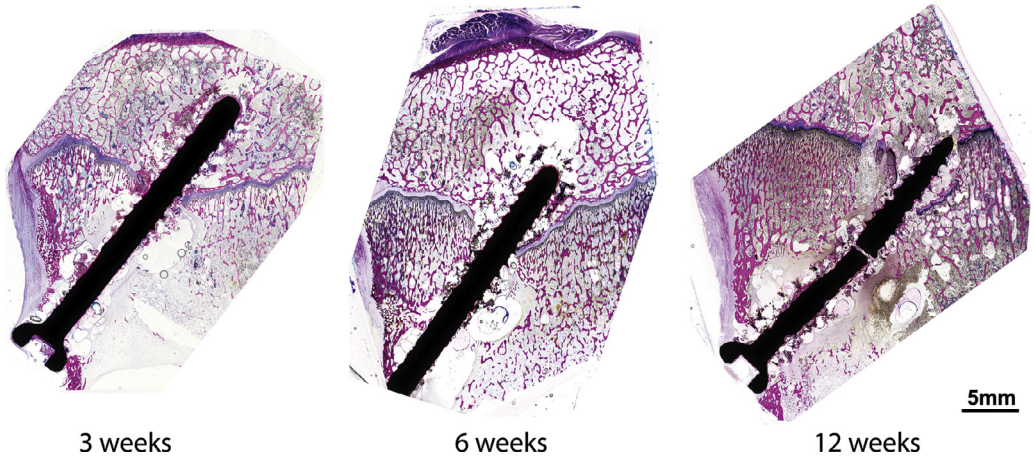

Fig. 13. Histological depiction of two intact (3 and 6 weeks) and one broken screw (in the 12-weeks group) with transepiphyseal position.

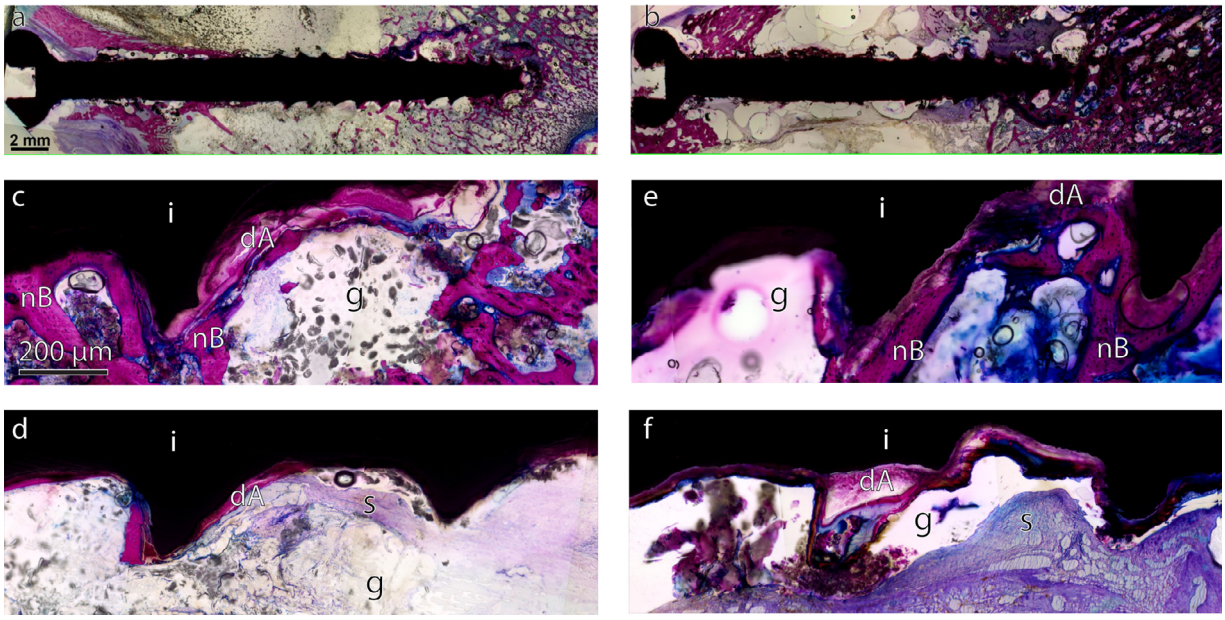

Fig. 14. Histological comparison of ZX00 screws in the control and fracture groups. Overview of the Mg screw after 12 weeks in (a) the control group and (b) the fracture group. The screws are preserved to a large extent. In the magnifications (c-f) of the overview images, the implant (i), degradation areas (dA), and gas pockets (g) surrounded by compressed soft tissue (s) are visible. New bone (nB) formed on the screw surfaces in tapestry-like layers. The scale bar in (a) is for (a) and (b); the scale bar in (c) is for (c-f). The slices were stained with a Methylene Blue and Basic Fuchsine combination.

significantly lower volume fraction of the Mg_2Ca phase in ZX00 at about 0.6% (Fig. 5) compared to 8.5% for XZ51 [62]. In fact, this phase was reported to reduce the tensile strength and to represent a potential nucleation point for crack formation [63] thus limiting ductility. Furthermore, the here reported elongation at fracture for ZX00 is in the range of titanium Grade 2 (about 20%) and somewhat higher than the significantly stronger Ti-6Al-4V alloy Grade 5 (10-15%) [66]. In summary, the mechanical data obtained demonstrate that we succeeded in reducing the Zn alloying content from 1 wt% in ZX10 to 0.45 wt% in ZX00 without compromising on the alloy's strength and with an acceptable compromise on the alloy's ductility.

As intended, the Zn reduction presumably caused the tendency towards a lower *in vitro* degradation rate for ZX00 compared to ZX10, as shown by the smaller gas-evolution rate (Fig. 7b). This matches the trend observed in previous studies, in that slower degradation rates were observed for decreasing Zn amounts: ZX50 (5.0 wt% Zn) > ZX20 (1.5 wt% Zn) > ZX10 (1.0 wt% Zn) [26,29]. The reduced degradation rate of ZX00 is explained by two mechanisms: first, in contrast to alloys containing > 1.0 wt% Zn, the microstructure of ZX00 was found to be free of the ternary phase IM1 ($Ca_3Mg_xZn_{15-x}$ with $4.6 \leq x \leq 12$) [37]), which is known to be cathodic to the Mg matrix [40] and is likely to accelerate degradation *in vitro* and *in vivo* [29]. In contrast, only the Mg_2Ca phase was found in the ZX00 alloy processed by hot extrusion (Fig. 6e). This phase behaves anodically, leading to slow and homogenous degradation when present in a moderate phase fraction [29, 38]. Furthermore, compared to ZX10, which also only contains the Mg_2Ca phase, ZX00's lower degradation rate may be explained by the lower Zn-solute content. Zn was recently found to redeposit on the surface of corroding Mg–Zn–Ca alloys and act as nano-cathodes, thus accelerating the Mg-matrix dissolution via nano-galvanic coupling [29].

The second major aim of the present study was to investigate the clinical applicability of screw osteosynthesis using the magnesium alloy ZX00 in a growing-sheep model, where osteotomized bone was compared to an intact control group regarding degradation behavior and fracture healing.

Concerning the implant volume, an initial rapid volume decrease of 9% within the first 3 weeks was observed for the proximal, monocortical screws close to the epiphyseal plate in the tibial plateau. Subsequently, the degradation almost stagnated up to 12 weeks *post operation*. The distal bicortical screws in the shaft area also showed an initially higher volume loss of 5% within the first 3 weeks and a further loss of 5% until 12 weeks *post operation*, giving an overall loss of 10% within 12 weeks.

The temporally different volume loss between the proximal screws surrounded with spongiose bone on all sides and the bicortically set screws in the shaft area, which pass through the medullary canal and protrude into the surrounding soft tissue at the end of the screw, can be ascribed to the presence of different tissue types surrounding the implant [39]. Mechanical forces acting on the musculature surrounding the bone-protruding implant may also add to an increased degradation rate. This phenomenon can be circumvented in the implant's clinical use in humans, in which the screw length is chosen individually to match the patient's anatomy.

Witte et al. described the generation of a direct contact between the Ca-phosphate-enriched corrosion-product layer around the implant and the surrounding tissue [35]. Any increase in volume after the initial decrease within the first 3 weeks, for both distal and proximal screws, is therefore most likely due to osseointegration of the implant and its subsequently reduced demarcation to the bone. This phenomenon appeared especially in the first weeks before the produced gas enhanced delineation. Neither the proximal nor the distal screws showed a significant difference between the fractured and non-fractured sides in terms of volume loss. The fracture or its healing process is therefore not expected to have an influence on the degradation behavior in terms of volume loss of the Mg screws.

The surface area of the proximal screws increased by 9.4% from the baseline to the 12th week, whereas that of the distal screws only showed an increase of 2.9%. Proximally, no difference was found between the right and left sides, while the distal screws on the left side increased in surface, especially between the 6th and 12th week, and those on the right side significantly reduced in surface during the same time interval.

The general increase in surface area between the initial situation and the 12th week, observed for both the proximal and the distal screws, indicates lateral heterogeneous corrosion attack of the implant [67]. On the other hand, the significant decrease in surface area between the 6th and 12th week on the osteotomized distal side, which correlates with a significant decrease in volume over the same time interval, may be due to an influence of the surrounding tissue, as described by Sanchez et al. [41]. In particular, the medullary canal located in the shaft area, which contains immunological cells and cytokines with corresponding chemotaxis, may influence the physiological fracture healing process, which in turn may influence the material degradation of the distal screws.

In any case, the osteotomy is accompanied by an inflammatory reaction and may thus be associated with accelerated degradation through the cofactor of the bone marrow. However, looking at the entire set of screws, a significant difference between the fracture and the reference side was not found, neither with respect to the overall volume loss nor with respect to the degradation of the proximal or distal parts. Therefore it must be concluded that the fracture healing process, including its influencing factors on the surrounding milieu, has no significant influence on the degradation behavior of ZX00 implants.

The gas volume, which forms as a consequence of Mg degradation as part of the electrochemical reaction along with the generation of magnesium hydroxide, showed a steady increase around the distal screws until the 12th week, while the gas volume around the proximal screws decreased up to the 6th week followed by an increase up to 12 weeks. A correlation between the fracture healing process and hydrogen gas volume could not be established, as there were no significant differences between the osteotomized and non-osteotomized sides. The gas-formation behavior is, however, likely to be different between the proximal screw at the cancellous bone and the distal screw at the medullary canal located in the shaft area due to the influence of the peri-implant environment.

Despite the chronologically different gas volumes between the proximal and distal screws, a complete consolidation of the osteotomy was found after 12 weeks in all animals investigated. The fracture and its impact on ZX00 degradation therefore appears to have no influence on fracture healing. Additionally, two screws were found broken at the time of examination (see Figs. 12 and 13). This purely observation-based finding underlines the great suitability of deploying Mg-based osteosynthesis screws for fracture stabilization in pediatric traumatology. The fracture is stabilized in the first weeks until bone healing is achieved, but the screws break when bone lengthening proceeds in the epiphyseal plate.

To date, one trial presents four cases regarding the implementation of REE-alloyed magnesium implants in adolescents. Pins and screws were used for flake fracture fixation and revealed promising results [68]. Furthermore, sixteen clinical trials on the implementation of REE-alloyed magnesium implants in adults have been reported [45-60]. The first clinical trials focused on metatarsal osteotomy fixation for the correction of hallux valgus deformities [49]. Apart from these promising results, poor outcomes were reported in two studies with extensive gas formation, loosening and cyst formation within carpal bones after scapho-trapezio-trapezoid (STT) fusion [45] and after acute scaphoid fracture fixation [46]. In addition, Lee et al. [61] tested in a single center trial the performance of Mg-5Ca-1Zn (in wt%) (XZ51), which is an Mg–Ca–Zn alloy with significantly larger Ca content (and thus Ca-to-Zn ratio) than in the alloy ZX00, in the treatment of hand fractures. A total of 53 cases with a follow-up over 12 months revealed excellent results without a single failure after 6 and 12 months post-implantation. None of the patients experienced a decline in grip power and the range of motion in the wrist joint remained unchanged.

However, with respect to clinical applicability, a crucial aspect of resorbable Mg implants must be considered. This concerns the widely discussed radiolucent zones around the implant caused by gas formation. In our research we have observed increased radiolucency to a certain degree, followed by a constant period and finally recurrent increase in density. This probably results from a higher endosteal bone mass at the region of gas accumulation around the screw over time. This observation-based finding of newly formed endosteal bone, visible as increased density in the radiolucent areas, is possibly caused by the osteoinductive effect of Mg screws, which thereby compensates for the negative impact of gas accumulation in the early stages. If hydrogen-gas evolution exceeds a certain limit, the radiolucent areas formed by trapped gas are at risk of forming encapsulated gas cavities, which are edged by a sclerotic line seen in radiographs. In our opinion, these encapsulated gas cavities are a pre-stage to persisting osteolysis and must be avoided. We did not observe loosening of any screws and no cystic encapsulation. Based on our preclinical testing, we expect the implants to completely dissolve within two years.

In our opinion, the size of the bone and its capacity to distribute the evolving gas plays an import role. Therefore we predict a higher risk for failure in small bones, caused by accumulation of trapped gas, as illustrated in recent literature [45,46].

There are some limitations to this study. The follow-up ended after achieving a complete consolidation of the bone at 12 weeks, so that we cannot make a statement with respect to the long-term outcome after complete dissolving of the implants. Further *in vivo* studies are therefore necessary to investigate long-term effects of gas-cavity formation around the implants until they completely dissolve. An *in vivo* trial should also focus on the impact of ZX00 on bone growth when screws are inserted through the physis.

5. Conclusions

This study demonstrates that reducing the Zn content of ZX10 to 0.45 wt% (0.17 at.%) and balancing the Ca content to 0.45 wt% (0.27 at.%) generates improved mechanical strength and a reduced *in vitro* degradation rate. *In vivo* experiments with ZX00 screws further reveal that all osteotomies completely consolidate after a maximum of 12 weeks. ZX00 screws exhibit a degradation behavior comparable to that of the control group and generate complete consolidation of osteotomized bone.

Declarations of Competing Interest

None.

Acknowledgements

The authors thank the Scientific Center for Optical and Electron Microscopy (ScopeM), ETH Zurich, for access to the instruments. We also thank Tatiana Akhmetshina and Sanjay Krishna Mohan for assistance with the thermodynamic calculations and EBSD imaging. The work was supported by the Swiss National Science Foundation (SNF Sinergia, Grant No. CRSII5- 180367) and the Laura Bassi Center of Expertise BRIC (Bioresorbable Implants for Children, FFG –Austria).

Role of the funding source

This research did not receive any specific grant from funding agencies in the public, commercial, or not-for-profit sectors.

References

[1] B.R. Olsen, A.M. Reginato, W. Wang, Bone development, Annu. Rev. Cell Dev. Biol. 16 (2000) 191–220.

[2] , Metallosis & Metal Poisoning: Hip Replacement Complications, DrugwatchCom, 2020 n.d. https://www.drugwatch.com/hip-replacement/metallosis/ (Accessed date: 26 December 2018).

[3] P. Thomas, M. Thomas, B. Summer, K. Dietrich, M. Zauzig, E. Steinhauser, V. Krenn, H. Arnholdt, M.J. Flaig, Impaired wound-healing, local eczema, and chronic inflammation following titanium osteosynthesis in a nickel and cobalt-allergic patient: a case report and review of the literature, J. Bone Joint Surg. Am. 93 (2011) e61.

[4] A.M. Weinberg, H. Tscherne, Unfallchirurgie: Unfallchirurgie im Kindesalter - Teil 1: Allgemeiner Teil, Kopf, Obere Extremität - Teil 2: Untere Extremität, Wirbelsäule, Körperhöhlen, Besonderheiten des kindlichen Skelettes, Springer, Berlin/Heidelberg, 2006.

[5] J. Nagels, M. Stokdijk, P.M. Rozing, Stress shielding and bone resorption in shoulder arthroplasty, J. Shoulder. Elbow. Surg. 12 (2003) 35–39.

[6] P. Augat, U. Simon, A. Liedert, L. Claes, Mechanics and mechano-biology of fracture healing in normal and osteoporotic bone, Osteoporos. Int. J. Establ. Result. Coop. Eur. Found. Osteoporos. Natl. Osteoporos. Found. USA 16 (Suppl 2) (2005) S36–S43.

[7] F. Marco, F. Milena, G. Gianluca, O. Vittoria, Peri-implant osteogenesis in health and osteoporosis, Micron 36 (2005) 630–644.

[8] W.R. Walsh, N.J. Cotton, P. Stephens, J.E. Brunelle, A. Langdown, J. Auld, F. Vizesi, W. Bruce, Comparison of poly-L-lactide and polylactide carbonate interference screws in an ovine anterior cruciate ligament reconstruction model, Arthroscopy 23 (2007) 757–765.

[9] U. Thormann, V. Alt, L. Heimann, C. Gasquere, C. Heiss, G. Szalay, J. Franke, R. Schnettler, K.S. Lips, The biocompatibility of degradable magnesium interference screws: an experimental study with sheep, BioMed Res. Int. (2015) (2015) 1–15 article ID 943603.

[10] T. Bizenjima, T. Takeuchi, F. Seshima, A. Saito, Effect of poly (lactide-co-glycolide) (PLGA)-coated beta-tricalcium phosphate on the healing of rat calvarial bone defects: a comparative study with pure-phase beta-tricalcium phosphate, Clin. Oral. Implants. Res. 27 (2016) 1360–1367.

[11] B. Zhao, X. Qiu, D. Wang, H. Li, X. He, Application of bioabsorbable screw fixation for anterior cervical decompression and bone grafting, Clinics 71 (2016) 320.

[12] N.G. Grün, P.L. Holweg, N. Donohue, T. Klestil, A.M. Weinberg, Resorbable implants in pediatric fracture treatment, Innov. Surg. Sci. 3 (2018) 119–125.

[13] B. León, J. Jansen (Eds.), Thin Calcium Phosphate Coatings for Medical Implants [Internet], Springer New York, New York, NY, 2009 [cited 2017 Oct 6]. Available from: http://link.springer.com/10.1007/978-0-387-77718-4 .

[14] J. Black, Biological Performance of Materials: Fundamentals of Biocompatibility, Fourth ed., CRC Press, 2005.

[15] L. Wu, F. Feyerabend, A.F. Schilling, R. Willumeit-Römer, B.J.C. Luthringer, Effects of extracellular magnesium extract on the proliferation and differentiation of human osteoblasts and osteoclasts in coculture, Acta. Biomater. 27 (2015) 294–304.

[16] K. Jähn, H. Saito, H. Taipaleenmäki, A. Gasser, N. Hort, F. Feyerabend, H. Schlüter, J.M. Rueger, W. Lehmann, R. Willumeit-Römer, E. Hesse, Intramedullary Mg_2Ag nails augment callus formation during fracture healing in mice, Acta. Biomater. 36 (2016) 350–360.

[17] Y. Zhang, J. Xu, Y.C. Ruan, M.K. Yu, M. O'Laughlin, H. Wise, D. Chen, L. Tian, D. Shi, J. Wang, S. Chen, J.Q. Feng, D.H. Chow, X. Xie, L. Zheng, L. Huang, S. Huang, K. Leung, N. Lu, L. Zhao, H. Li, D. Zhao, X. Guo, K. Chan, F. Witte, H.C. Chan, Y. Zheng, L. Qin, Implant-derived magnesium induces local neuronal production of CGRP to improve bone-fracture healing in rats, Nat. Med. 22 (2016) 1160–1169.

[18] M. Cheng, T. Wahafu, G.G. Jiang, W. Liu, Y.Q. Qiao, X.C. Peng, T. Cheng, X.L. Zhang, G. He, X.Y. Liu, A novel open-porous magnesium scaffold with controllable microstructures and properties for bone regeneration, Sci. Rep. 6 (2016) 24134.

[19] P. Makkar, S.K. Sarkar, A.R. Padalhin, B.-G. Moon, Y.S. Lee, B.T. Lee, In vitro and in vivo assessment of biomedical Mg–Ca alloys for bone implant applications, J, Appl. Biomater. Funct. Mater. 16 (2018) 126–136.

[20] K. Pichler, T. Kraus, E. Martinelli, P. Sadoghi, G. Musumeci, P.J. Uggowitzer, A.M. Weinberg, Cellular reactions to biodegradable magnesium alloys on human growth plate chondrocytes and osteoblasts, Int. Orthop. 38 (2014) 881–889.

[21] A. Myrissa, S. Bräuer, E. Martinelli, R. Willumeit-Römer, W. Gössler, A.M. Weinberg, Gadolinium accumulation in organs of Sprague–Dawley® rats after implantation of a biodegradable magnesium-gadolinium alloy, Acta. Biomater. 48 (2017) 521–529.

[22] A. Myrissa, A. Nezha Ahmad, Y. Lu, E. Martinelli, J. Eichler, G. Szakacs, C. Kleinhans, R. Willumeit-Römer, U. Schäfer, A.M. Weinberg, In vitro and in vivo comparison of binary Mg alloys and pure Mg, Mater. Sci. Eng. C. Mater. Biol. Appl. 61 (2016) 865–874.

[23] F. Amerstorfer, S. Fischerauer, L. Fischer, J. Eichler, J. Draxler, A. Zitek, M. Meischel, E. Martinelli, T. Kraus, S. Hann, S.E. Stanzl-Tschegg, P.J. Uggowitzer, J.F. Löffler, A.M. Weinberg, T. Prohaska, Long-term *in vivo* degradation behavior and near-implant distribution of resorbed elements for magnesium alloys WZ21 and ZX50, Acta. Biomater. 42 (2016) 440–450.

[24] L. Jin, J. Wu, G. Yuan, T. Chen, In vitro study of the inflammatory cells response to biodegradable Mg-based alloy extract, PLoS. One. 13 (2018) e0193276.

[25] S. Hirano, K.T. Suzuki, Exposure, metabolism, and toxicity of rare earths and related compounds, Environ. Health. Perspect. 104 (Suppl 1) (1996) 85–95.

[26] J. Hofstetter, M. Becker, E. Martinelli, A.M. Weinberg, B. Mingler, H. Kilian, S. Pogatscher, P.J. Uggowitzer, J.F. Löffler, High-strength low-alloy (HSLA) Mg–Zn–Ca alloys with excellent biodegradation performance, JOM 66 (2014) 566–572.

[27] J. Hofstetter, S. Rüedi, I. Baumgartner, H. Kilian, B. Mingler, E. Povoden-Karadeniz, S. Pogatscher, P.J. Uggowitzer, J.F. Löffler, Microstructure–property relations of high-strength low-alloy (HSLA) Mg–Zn–Ca alloys, Acta. Mater. 98 (2015) 423–432.

[28] S. Jafari, R.K. Singh Raman, C.H.J. Davies, J. Hofstetter, P.J. Uggowitzer, J.F. Löffler, Stress corrosion cracking and corrosion fatigue characterisation of MgZn1Ca0.3 (ZX10) in a simulated physiological environment, J. Mech. Behav. Biomed. Mater. 65 (2017) 634–643.

[29] M. Cihova, E. Martinelli, P. Schmutz, A. Myrissa, R. Schäublin, A.M. Weinberg, P.J. Uggowitzer, J.F. Löffler, The role of zinc in the biocorrosion behavior of resorbable Mg–Zn–Ca alloys, Acta. Biomater. 100 (2019) 398–414.

[30] N.G. Grün, P. Holweg, S. Tangl, J. Eichler, L. Berger, J.J.J.P. van den Beucken, J.F. Löffler, T. Klestil, A.M. Weinberg, Comparison of a resorbable magnesium implant in small and large growing-animal models, Acta. Biomater. 78 (2018) 378–386.

[31] T. Kraus, S.F. Fischerauer, A.C. Hänzi, P.J. Uggowitzer, J.F. Löffler, A.M. Weinberg, Magnesium alloys for temporary implants in osteosynthesis: in vivo studies of their degradation and interaction with bone, Acta. Biomater. 8 (2012) 1230–1238.

[32] J. Löffler, P. Uggowitzer, C. Wegmann, M. Becker, H. Feichtinger, Process and apparatus for vacuum distillation of high-purity magnesium. Patent EP2804964B1 (2019) and US9677151B2 (2017).

[33] G. Song, A. Atrens, D. St John, An hydrogen evolution method for the estimation of the corrosion rate of magnesium alloys, in: J.N. Hryn (Ed.), Magnesium Technology 2001, TMS, New Orleans, LA, USA, 2001, pp. 254–262.

[34] J. Hofstetter, E. Martinelli, A.M. Weinberg, M. Becker, B. Mingler, P.J. Uggowitzer, J.F. Löffler, Assessing the degradation performance of ultrahigh-purity magnesium *in vitro* and *in vivo*, Corr. Sci. 91 (2015) 29–36.

[35] F. Witte, V. Kaese, H. Haferkamp, E. Switzer, A. Meyer-Lindenberg, C. Wirth, H. Windhagen, In vivo corrosion of four magnesium alloys and the associated bone response, Biomater. 26 (2005) 3557–3563.

[36] P.K. Bowen, J. Drelich, J. Goldman, Magnesium in the murine artery: Probing the products of corrosion, Acta Biomater. 10 (2014) 1475–1483.

[37] Y.N. Zhang, D. Kevorkova, J. Li, E. Essadiqi, M. Medraj, Determination of the solubility range and crystal structure of the Mg-rich ternary compound in the Ca-Mg-Zn system, Intermetallics 18 (2010) 2404–2411.

[38] D. Zander, N.A. Zumdick, Influence of Ca and Zn on the microstructure and corrosion of biodegradable Mg-Ca-Zn alloys, Corr. Sci. 93 (2015) 222–233.

[39] C. Rössig, N. Angrisani, P. Helmecke, S. Besdo, J.M. Seitz, B. Welke, N. Fedchenko, H. Kock, J. Reifenrath, In vivo evaluation of a magnesium-based degradable intramedullary nailing system in a sheep model, Acta Biomater. 25 (2015) 369–383.

[40] M. Cihova, P. Schmutz, R. Schäublin, J.F. Löffler, Biocorrosion Zoomed In, Biocorrosion Zoomed In: Evidence for Dealloying of Nanometric Intermetallic Particles in Magnesium Alloys, Adv. Mater. 31 (42) (2019) 1903080 1903080.

[41] A.H.M. Sanchez, B.J.C. Luthringer, F. Feyerabend, R. Willumeit, Mg and Mg alloys: how comparable are in vitro and in vivo corrosion rates? A review, Acta Biomater. 13 (2015) 16–31.

[42] CompuTherm LLC, Pandat software package for calculating phase diagrams and thermodynamic properties of multi-component alloys, Madison, USA, www.computherm.com.

[43] MatCalc software package for computer simulation of phase transformation and microstructure evolution in metallic systems, Vienna, Austria, www.matcalc-engineering.com.

[44] Y.-N. Zhang, D. Kevorkov, F. Bridier, M. Medraj, Experimental study of the Ca-Mg-Zn system using diffusion couples and key alloys, Sci. Technol. Adv. Mater. 12 (2011) 025003.

[45] A. Wichelhaus, J. Emmerich, T. Mittlmeier, A case of implant failure in partial wrist fusion applying magnesium-based headless bone screws, Case Rep. Orthop. (2016) 7049130.

[46] R. Meier, M. Panzica, First results with a resorbable MgYREZr compression screw in unstable scaphoid fractures show extensive bone cysts, Handchir. Mikrochir. Plast. Chir. 49 (2017) 37–41.

[47] R. Biber, J. Pauser, M. Geßlein, H.J. Bail, Magnesium-based absorbable metal screws for intra-articular fracture fixation, Case Rep. Orthop. (2016) 9673174.

[48] A Turan, YA Kati, B Acar, O Kose, Magnesium bioabsorbable screw fixation of radial styloid fractures: case report, J. Wrist. Surg. 9 (2020) 150–155.

[49] C. Plaass, C. von Falck, S. Ettinger, L. Sonnow, F. Calderone, A. Weizbauer, J. Reifenrath, L. Claassen, H. Waizy, K. Daniilidis, C. Stukenborg-Colsman, H. Windhagen, Bioabsorbable magnesium versus standard titanium compression screws for fixation of distal metatarsal osteotomies - 3 year results of a randomized clinical trial, J. Orthop. Sci. 23 (2018) 321–327.

[50] H. Windhagen, K. Radtke, A. Weizbauer, J. Diekmann, Y. Noll, U. Kreimeyer, R. Schavan, C. Stukenborg-Colsman, H. Waizy, Biodegradable magnesium-based screw clinically equivalent to titanium screw in hallux valgus surgery: short term results of the first prospective, randomized, controlled clinical pilot study, Biomed. Eng. Online 12 (2013) 62.

[51] C. Plaass, S. Ettinger, L. Sonnow, S. Koenneker, Y. Noll, A. Weizbauer, J. Reifenrath, L. Claassen, K. Daniilidis, C. Stukenborg-Colsman, H. Windhagen, Early

results using a biodegradable magnesium screw for modified chevron osteotomies, J. Orthop. Res. 34 (2016) 2207–2214.
[52] H. Leonhardt, A. Franke, N.M.H. McLeod, G. Lauer, A. Nowak, Fixation of fractures of the condylar head of the mandible with a new magnesium-alloy biodegradable cannulated headless bone screw, Br. J. Oral Maxillofac. Surg. 55 (2017) 623–625.
[53] R. Biber, J. Pauser, M. Brem, H.J. Bail, Bioabsorbable metal screws in traumatology: a promising innovation, Trauma Case Rep 8 (2017) 11–15.
[54] O. Kose, A. Turan, M. Unal, B. Acar, F. Guler, Fixation of medial malleolar fractures with magnesium bioabsorbable headless compression screws: short-term clinical and radiological outcomes in eleven patients, Arch. Orthop. Trauma Surg. 138 (2018) 1069–1075.
[55] B. Acar, O. Kose, A. Turan, M. Unal, Y.A. Kati, F. Guler, Comparison of bioabsorbable magnesium versus titanium screw fixation for modified distal chevron osteotomy in hallux valgus, Biomed. Res. Int. 19 (2018) 5242806.
[56] J.T. Choo, S.H.S. Lai, C.Q.Y. Tang, G. Thevendran, Magnesium-based bioabsorbable screw fixation for hallux valgus surgery - a suitable alternative to metallic implants, Foot Ankle Surg. S1268-7731 (2018) 30392–30398.
[57] H. Klauser, Internal fixation of three-dimensional distal metatarsal I osteotomies in the treatment of hallux valgus deformities using biodegradable magnesium screws in comparison to titanium screws, Foot Ankle Surg. S1268-7731 (2018) 30030–30034.
[58] A. Gigante, N. Setaro, M. Rotini, S.S. Finzi, M. Marinelli, Intercondylar eminence fracture treated by resorbable magnesium screws osteosynthesis: a case series, Injury. 49 (Suppl 3) (2018) S48–S53.
[59] B. Acar, M. Unal, A. Turan, O. Kose, Isolated lateral malleolar fracture treated with a bioabsorbable magnesium compression screw, Cureus 10 (2018) e2539.
[60] C. Aktan, M.B. Ertan, A. Turan, O. Kose, Fixation of small osteochondral fragments in a comminuted distal humerus fracture with magnesium bioabsorbable screws: a case report, Cureus 10 (2018) e3752.
[61] J.W. Lee, H.S. Han, K.J. Han, J. Park, H. Jeon, M.R. Ok, H.K. Seok, J.P. Ahn, K.E. Lee, D.H. Lee, S.J. Yang, S.Y. Cho, P.R. Cha, H. Kwon, T.H. Nam, J.H. Han, H.J. Rho, K.S. Lee, Y.C. Kim, D. Mantovani, Long-term clinical study and multiscale analysis of in vivo biodegradation mechanism of Mg alloy, Proc. Natl. Acad. Sci. USA 113 (2016) 716–721.
[62] P.R. Cha, H.S. Han, G.F. Yang, Y.C. Kim, K.H. Hong, S.C. Lee, J.Y. Jung, J.P. Ahn, Y.Y. Kim, S.Y. Cho, J.Y. Byun, K.S. Lee, S.J. Yang, H.K. Seok, Biodegradability engineering of biodegradable Mg alloys: tailoring the electrochemical properties and microstructure of constituent phases, Sci. Rep. 3 (2013) 2367.
[63] E. Zhang, L. Yang, Microstructure, mechanical properties and bio-corrosion properties of Mg–Zn–Mn–Ca alloy for biomedical application, Mater. Sci. Eng. 497 (2008) 111–118.
[64] E. Hall, The deformation and ageing ofmild steel: III discussion of results, Proc. Phys. Soc. Sec. B 64 (9) (1951) 747 N.J. Petch, The cleavage strength of polycrystals, J. Iron and Steel Inst. 174 (1953) 25e28.
[65] K. Huang, R.E. Logé, A review of dynamic recrystallization phenomena in metallic materials, Mater. Des. 111 (2016) 548–574.
[66] N. Mitsuo, Mechanical properties of biomedical titanium alloys, Mater. Sci. Eng. A 243 (1998) 231–236.
[67] S.F. Fischerauer, T. Kraus, X. Wu, S. Tangl, E. Sorantin, A.C. Hänzi, J.F. Löffler, P.J. Uggowitzer, A.M. Weinberg, In vivo degradation performance of micro-arc-oxidized magnesium implants: a micro-CT study in rats, Acta Biomater. 9 (2013) 5411–5420.
[68] M. Rupprecht, M. Kertai, Erste Ergebnisse mit magnesiumbasierten Implantaten im Kindes- und Jugendalter, Jatros Orthopädie & Traumatologie Rheumatolgie (2/2019).

Follow us @BoneJointRes

Freely available online OPEN ACCESS

BJR

BIOMATERIALS

A Lean Bioabsorbable Magnesium-Zinc-Calcium Alloy ZX00 Used for Operative Treatment of Medial Malleolus Fractures: Early Clinical Results of A Prospective Non-Randomized First in Man Study

P. Holweg,
V. Herber,
M. Ornig,
G. Hohenberger,
N. Donohue,
P. Puchwein,
A. Leithner,
F. Seibert

Aims

This study is a prospective, non-randomized trial for the treatment of fractures of the medial malleolus using lean, bioabsorbable, rare-earth element (REE) free, magnesium (Mg)-based biodegradable screws in the adult skeleton.

Methods

A total of 20 patients with isolated, bimalleolar, or trimalleolar ankle fractures were recruited between July 2018 and October 2019. Fracture reduction was achieved through bioabsorbable Mg-based screws composed of pure Mg alloyed with zinc (Zn) and calcium (Ca) (0.45 wt% Zn and 0.45 wt% Ca; ZX00). Visual analogue scale (VAS) and the presence of complications (adverse events) during follow-up (12 weeks) were used to evaluate the clinical outcomes. The functional outcomes were analyzed through the range of motion (ROM) of the ankle joint and the American Orthopaedic Foot and Ankle Society (AOFAS) score. Fracture reduction and gas formation were assessed using several plane radiographs.

Results

The follow-up was performed after at least 12 weeks. The mean difference in ROM of the talocrural joint between the treated and the non-treated site decreased from 39° (SD 12°) after two weeks to 8° (SD 11°) after 12 weeks ($p \leq 0.05$). After 12 weeks, the mean AOFAS score was 92.5 points (SD 4.1). Blood analysis revealed that Mg and Ca were within a physiologically normal range. All ankle fractures were reduced and stabilized sufficiently by two Mg screws. A complete consolidation of all fractures was achieved. No loosening or breakage of screws was observed.

Conclusion

This first prospective clinical investigation of fracture reduction and fixation using lean, bioabsorbable, REE-free ZX00 screws showed excellent clinical and functional outcomes.

Cite this article: *Bone Joint Res* 2020;9(8):xxx–xxx.

Keywords: Lean magnesium screws, Rare-earth elements, Ankle fractures, Functional outcome

Article focus

- First prospective clinical evaluation of a lean Magnesium-Zinc-Calcium Alloy ZX00 screw.
- Clinical and radiological outcome after fracture stabilization of the medial malleolus with ZX00.

Key messages

- Biodegradable magnesium implant without any rare-earth elements.
- Unimpeded fracture healing in all patients despite small radiolucency during the first 12 weeks around the screw.
- No postoperative adverse events.

Correspondence should be sent to Valentin Herber; email: valentin.herber@medunigraz.at

doi: 10.1302/2046-3758.98.BJR-2020-0017.R2

Bone Joint Res 2020;9(8):xxx–xxx.

Strengths and limitations

- Prospective study including20 patients.
- Ethically prohibited control group.
- Early results only: the follow-up for all patients was at least 12 weeks.

Introduction

Medial malleolar fractures are very common among the adult population and constitute approximately 9% of all fractures.[1] Current literature recommends operative treatment of ankle fractures through open reduction and internal fixation,[2] followed by immobilization and rehabilitation.[3-6] Many different approaches are described for fixation of medial malleolus fractures, including screw-only fixation and using plates in combination with screws.[7] The most commonly employed and accepted clinical technique is the operative fixation of medial malleolar fractures with cancellous screws.[8] A recent trial recommended a single screw for fixation of the medial malleolar fracture, with equivalent mid-term patient outcomes, compared to double screw fixation.[9] Especially in older patients, conservative treatment with close contact casting is an equivalent therapy in terms of functional outcomes at long-term follow-up, although careful monitoring in the weeks after its application to monitor the maintenance of reduction is required.[10]

Nevertheless, many patients report postoperative dissatisfaction due to persistent pain. In most cases, the cause of this pain is a soft-tissue irritation resulting from hardware placement, or a shoe. In some circumstances, a patient's pain might be severe enough to require hardware removal.[7]

Over the last decade, there has been an increasing demand to overcome these disadvantages associated with conventional implant materials, by developing new, alternative materials and material production approaches for use in trauma care.[11,12] Among biodegradable metals, magnesium (Mg)-based implants exhibit good biocompatibility and suitable biomechanical properties, with appropriate mechanical strength and ductility, providing an advantage over biodegradable polymers and ceramics.[13-15] Recently, considerable efforts have been made to reduce the Mg- degradation rate,[16,17] to inhibit excess hydrogen gas evolution and encapsulated gas cavities.[18,19] One of these strategies is the use of rare-earth elements (REE), such as yttrium or gadolinium, to decelerate degradation.[20,21] Mg- based implants alloyed with REE, however, were observed to induce apoptosis and necrosis with high-concentration extracts. Furthermore, a negative effect on the viability of immune cells *in vitro* was documented.[22]

Therefore, in cooperation with ETH Zurich (Switzerland) we transitioned to lean Mg-based implant materials (ZX00) alloyed with zinc (Zn) and calcium (Ca),[23] without any REE, to avoid both short-term and crucially, long-term adverse effects.

Grün et al[24] demonstrated the degradation performance of this material termed ZX00 (Mg-Zn0.45-Ca0.45, in wt.%) in a small and large growing-animal model study and reported no negative effects on bone formation and ingrowth. ZX00 showed slow and homogeneous degradation.[24]

Facing Mg-based implants, the elementary questions of implant loosening caused by gas evolution and long-term result of the radiolucent zones have to be considered.

To date, there are no prospective investigations that elaborate on these findings.

Based on these aspects, we planned this prospective, non-randomized first in man study to evaluate the safety and the early clinical and functional outcomes of lean, REE-free, Mg compression screws (ZX00) in the case of fracture stabilization of the medial malleolus in humans.

Methods

The pilot study was designed as a prospective, non-randomized trial for the treatment of displaced fractures of the medial malleolus with a lean, REE-free, Mg-based biodegradable implant in the adult skeleton. The trial was conducted according to the Good Clinical Practice (ISO 14155:2011) standard and the Declaration of Helsinki.

Patient enrolment. The study was performed at the Department of Orthopaedics and Trauma at our institution and approved by the ethics committee (28 to 071 ex 15/16). A total of 20 subjects were recruited and operated on by three experienced surgeons in the centre between July 2018 and October 2019. The follow-up timepoint for all patients was at least 12 weeks. Inclusion focused on adults aged between 18 and 65 years presenting with a displaced isolated medial malleolus fracture, a bimalleolar ankle fracture, or a trimalleolar ankle fracture. Fracture displacement was defined as diastasis of the fracture in any direction of 2 mm or more. Exclusion criteria were pathological fractures, underlying diseases (particularly bone diseases, kidney diseases, diabetes mellitus), polytraumatized patients, and pregnant or breastfeeding women.

Written informed consent was obtained from each patient before the surgery. Standardized electronic case report forms (eCRFs) were used to collect individual patient data during this study. All radiological data were stored in a picture archiving and communication system (PACS). Fractures were classified according to the Herscovici system.[25]

Bioabsorbable devices. Ultra-high pure Mg (99.999%) was alloyed with Zn and Ca (0.45 wt% Zn and 0.45 wt% Ca) at 750°C under a protective gas atmosphere. This alloy was produced by ETH Zürich in cooperation with de Cavis AG (Swiss Federal Laboratories for Materials Science and Technology, Dübendorf, Switzerland). The extrusion of the material into 6 mm rods was accomplished by LKR Leichtmetallkompetenzzentrum Ranshofen (Ranshofen, Austria; certified to ISO 9001:2008) and

Table I. Patient follow-up, assessments, and visits.

Study visit per patient	Baseline	Operation	Dismissal	2 weeks (± 4 days)	6 weeks (± 4 days)	12 weeks (± 4 days)
Visit number	V1	V2	V3	V4	V5	V6
Inclusion/exclusion criteria	X					
Signed informed consent	X					
Demographics	X					
Relevant medical history	X					
Laboratory/urinary analysis	X				X	X
Radiograph (two plane)	X	X	X	X	X	X
Range of motion (ROM) (standard goniometer)				X	X	X
Clinical examination			X	X	X	X
Wound (pain, redness, secretion, erythema)			X	X	X	X
Visual Analogue Scale (VAS)	X		X	X	X	X
AOFAS						X

AOFAS, American Orthopaedic Foot and Ankle Society.

compression screws were produced by Mattig Präzision GmbH (Obertrum am See, Austria; certified to ISO 9001:2008) in Graz. Packaging and sterilization by γ irradiation were performed by Biegler (Mauerbach, Austria) and Mediscan GmbH & Co KG (Kremsmünster, Austria; certified to EN ISO 13485 and ISO 11137, respectively). Prepared screws had a length of 40 mm and a diameter of 3.5 mm. Implants were threaded at the distal part for use as traction screws.

Surgery. All patients were operated in a supine position. In case of a bimalleolar or trimalleolar fracture, the fibular and the dorsal tibial fragments were treated before the medial malleolus. Subsequently, two parallel Kirschner wires perpendicular to the medial malleolar fracture line were positioned with fluoroscopic control. A cannulated drill bit with 2.7 mm width was used for preparing the hole. Subsequently, one wire was removed and the ZX00 compression screw was inserted into the hole. Final fixation of the fracture was achieved with the second bioabsorbable Mg screw after removal of the second wire. The insertion torque of the screws was limited at a force of 1.5 newton metre with a torque handle. In all patients, no additional implants other than the Mg screws were used for the fixation of the medial malleolus. Patients with bimalleolar fractures and trimalleolar fractures were fixed with titanium plates and screws. Moreover, patients were immobilized with an under-knee plaster cast four to six weeks postoperatively and encouraged to attempt full weight-bearing as tolerated. Ankle movement exercises were started immediately after removal of the plaster.

Assessments and measurements. For each subject, the study consisted of assessments conducted preoperatively, immediately after operation and postoperative follow-up visits (Table I). During follow-up, complications including vital signs, erythema, swelling, pain, secretions, wound healing disorders, wound infections, or implant infections were recorded. Pain was assessed using visual analogue scale (VAS). Blood analysis and detection of Ca and Mg were recorded. Functional outcomes were evaluated through range of motion (ROM) in dorsal and plantar flexion. Additionally, the American Orthopaedic Foot and Ankle Society (AOFAS) score[26] was performed after three months. Anteroposterior and lateral ankle radiographs (X-rays) were used to evaluate the fracture union and loss of reduction during follow-up. Postoperative radiograph evaluation was performed by two independent radiologists after surgery and after two, six, and 12 weeks. Fracture reduction and persisting gap or step were examined.

Statistical analysis. A descriptive analysis of the data was performed using proportions, frequency distributions, means, and standard deviations. Data were presented as the mean (SD). Comparisons between timepoints were assessed using a paired *t*-test. A p-value less than or equal to 0.05 was considered statistically significant.

Results

Patient information

Demographic data. A total of 20 patients were enrolled in the study (11 males and 9 females with a mean age of 40.1 years (SD 14.5)) between July 2018 and October 2019. The follow-up timepoint for all patients was at least 12 weeks. Patient demographics are shown in Table II.

During the first screening of the patients, every patient presented with normal vital signs and electrocardiograms (ECGs) were normal.

Aetiology and fracture classification. Ankle sprains caused 45% of all fractures. The rest were attributed to sports injuries (cycling, soccer, climbing, and skiing accidents). Four patients presented with traffic-related injuries (20%): two subjects (10%) had a bicycle accident, while one had a motor bike accident and another a car accident. According to the position of the medial malleolar fracture, 13 patients had a fracture type C Hercovici,

Table II. Patient demographics.

Demographic	Data
Mean age, yrs (SD)	40.1 (14.5)
Mean height, cm (SD)	171 (14)
Mean weight, kg (SD)	79.05 (9.92)
Mean body mass index (BMI), kg/m² (SD)	26.25 (2.25)

to 8° (SD 11°) after 12 weeks (Figure 2). There was a statistically significant difference between weeks 2 and 6 ($p \leq 0.05$) and between weeks 6 and week 12 ($p \leq 0.001$) concerning the difference of the total movement of the talocrural joint. At the final follow-up, the mean AOFAS score was 92.5 points (SD 4.1), which represents an excellent result for all patients. None of the patients showed

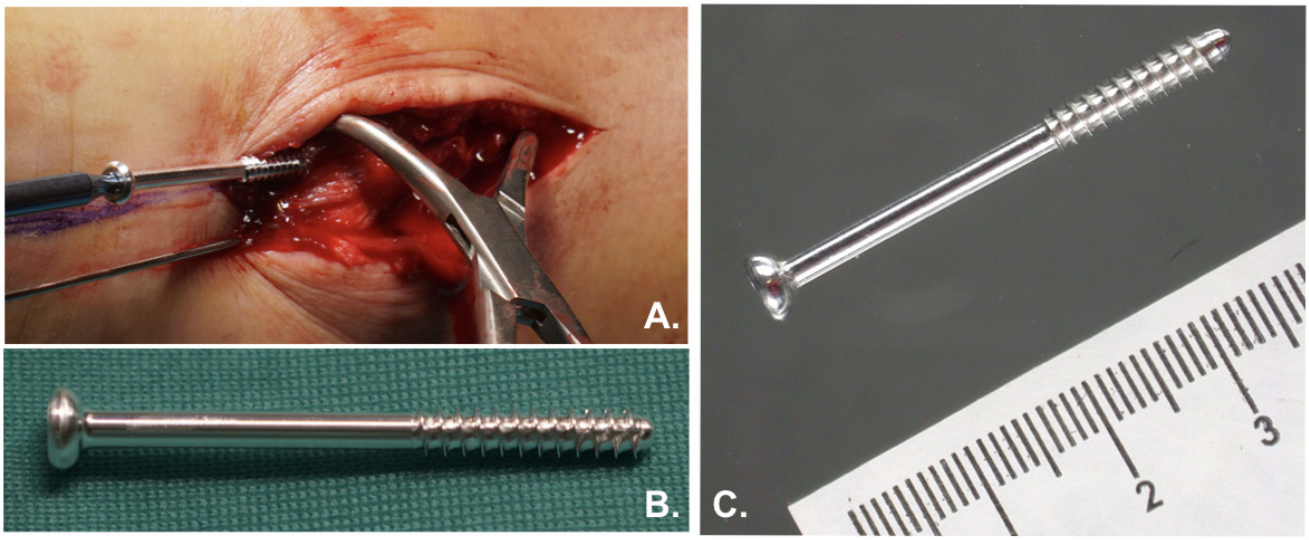

Fig. 1

a) Placement of a ZX00 screw in the medial malleolar during surgery. b) and c) External appearance of ZX00 screw.

six patients had a type B fracture, and one patient had a type A fracture.

Surgery and intraoperative outcomes. During surgery, all Mg-based screws were fixed successfully (Figure 1) and no intraoperative complications (including screw fracture) were observed. Most of the patients (60%) had an anatomical intraoperative reduction without any diastasis or gap. In total, 35% of the patients had a persisting gap of 1 mm and one patient had a fracture reduction with a persisting diastasis of more than 1 mm. Moreover, after surgery one unplanned CT scan analysis, performed because of debatable reduction, showed a persisting gap of 2 mm. None of the patients included in this study required unscheduled revision.

Clinical and functional outcomes. After surgery, the mean VAS was 1.6 points (SD 0.6) and 1.3 points (SD 0.5) after two weeks. Six weeks after surgery, all patients reported no pain (VAS 1) regarding the medial malleolus. Blood analysis and specifically the dosage of Mg and Ca were normal at all follow-up visits in the 20 patients with a Mg concentration between 0.700 mmol/l and 1.100 mmol/l and a Ca concentration between 2.20 mmol/l and 2.65 mmol/l. Moreover, renal function remained stable. The mean difference of the total movement of the talocrural joint (dorsal flexion/plantar flexion) between the operated site and the nonoperated site was 39° (SD 12°) after two weeks, 22° (SD 13°) after six weeks, and decreased wound healing disorders. None of the patients showed erythema, swelling, deep wound infections, or implant site infections. There was no loosening of the implant as a result of gas evolution.

After anteroposterior and lateral radiograph analysis, the ankle fracture was healed in 18 patients (90%) after six weeks. After 12 weeks, all patients showed complete consolidation of the ankle fractures. Serial radiographs displayed small radiolucent zones around the screws, increasing up to week 6, with a constant period to week 12, followed by a decrease to week 24. Despite this gas formation around the screws, no encapsulation was detected. In one patient, a CT scan was performed after 52 weeks, because of uncertainty of appropriate distal tibiofibular reduction after evaluation of the radiographs. Here, a screw volume loss of about 50% was displayed. Additionally an increased endosteal bone mass at the screw head was detected (Figure 3).

In one patient, a manifest osteoporosis was noticed before surgery. Compared to the other patients, an increased gas formation was seen around the screws (Figure 4). Nevertheless, bone healing was accomplished after six weeks. At this timepoint, a small sclerotic line could be detected at the border of the radiolucent zone to the surrounding tissue. Regardless, an increase in

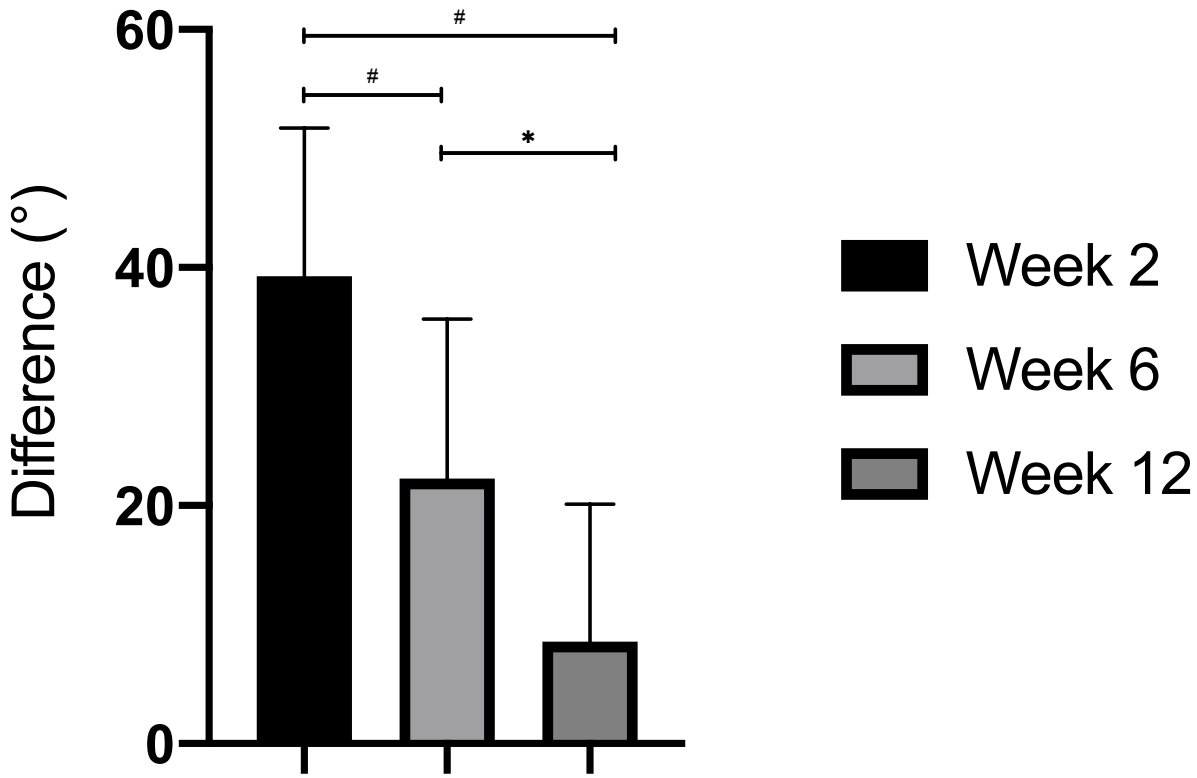

Fig. 2

Difference of the total movement of the talocrural joint between the operated site and the nonoperated site. * $p < 0.05$ and # $p < 0.001$.

density in this area due to higher endosteal bone mass at the region of expressed gas at the screw could be presented in the radiographs taken after 24 and 52 weeks of follow-up (Figures 3-4).

Discussion

To date, 16 clinical studies and case reports have been conducted for the clinical implementation of Mg implants alloyed with REE.[27–42] The earliest clinical trials on metatarsal osteotomy fixation for the correction of hallux valgus deformities[31–33] showed similar complications compared to titanium implants. Subsequently, good results were achieved for ankle fracture fixation and intra-articular fragment fixation.[29]

Apart from these promising results, poor outcomes have been reported in two studies with extensive gas formation, loosening and cystic formation within carpal bones after scapho-trapezio-trapezoid (STT) fusion[27] and secondarily after acute scaphoid fracture fixation.[28]

In our opinion, the size of the bone and its capacity to distribute the evolving gas plays an import role. Therefore, we expect a higher risk of failure in small bones, caused by the accumulation of entrapped gas, as illustrated in recent literature.[27,28]

This is the first implementation of the lean, REE-free Mg implant ZX00 in humans. Evaluation was performed by a prospective clinical investigation on functional and radiological results of medial malleolus fracture fixation with these implants. The promising results of this study demonstrate an adequate fixation of medial malleolus fractures using REE-free Mg screws ZX00. Despite the radiolucent areas around the screws at the first 12 weeks after implantation, all fractures healed without secondary displacement or implant breakage.

Increased gas formation was seen around the screws in one patient with a manifest osteoporosis. To our knowledge, metabolic and immunological changes due to osteoporotic disease can cause an increased degradation of Mg implants with expanded gas volume, seen as radiolucent areas. However, further investigations should focus on this highly sensitive elderly patient collective to understand the importance and underlying mechanism of osteoporosis in combination with Mg implants. Nevertheless, bone healing was accomplished in this patient after six weeks. Astonishingly, an obvious increase in

Fig. 3

a) Anteroposterior and lateral ankle radiographs of a 49-year-old female patient; medial malleolar fracture combined with distal tibiofibular joint disruption (Maisonneuve Fracture). b) Two weeks timepoint radiographs, anatomical reduction with two magnesium (Mg)-based screws and one titanium screw; visible fracture line at the medial malleolus, small signs of radiolucent zones within the bone surrounding the screws. c) Six weeks timepoint, plane radiographs with complete fracture consolidation, increase of radiolucent zones within the bone surrounding the screws, removed titanium screw. d) Timepoint radiograph images at 12 weeks with constant radiolucent zones. e) Timepoint radiographs at 24 weeks, f) CT scan at 52 weeks, decrease of radiolucent zones, increased endosteal bone mass, and periosteal bone ingrowth at the screw head (white arrow).

Fig. 4

Anteroposterior ankle radiographs of a 61-year-old female patient with pre-existing osteoporosis, bimalleolar fracture with a posterior malleolar fragment. From left to right, anteroposterior ankle radiograph after surgery, after two weeks (reduction of the fractures with two magnesium (Mg)-based screws and a titanium plate and screws), after six weeks (obvious radiolucent zones fracture consolidation), after 12 weeks (steady radiolucency, small sclerotic line at the border of the radiolucent zone to the surrounding tissue.), after 24 weeks, and after 52 weeks (steady sclerotic line, increase in density at former radiolucent area). The white arrows showed the gas formation arround the screw.

density at the radiolucent area within the sclerotic line was observed in the CT scan after 52 weeks. In our opinion, this finding of newly formed endosteal bone mass demonstrates the osteoinductive effect of the Mg screws, which compensates for the negative impact of gas expression in early stages.

Finally, this study will be extended for up to two years to visualize the expected complete degradation of the material and a full conversion of the radiolucent zones formed by expressed gas, into newly formed endosteal bone mass. Additionally, measurements of long-term functional outcomes will be performed.

There are some limitations to this study. Since this is the first implementation of this new, REE-free Mg material (ZX00) in humans, a control group was ethically not permissible. However, 20 patients were included in the study and visited at least until bone healing was achieved.

In conclusion, this investigation aimed to study the performance and safety of a new, REE-free material. Therefore, vital parameters as well as laboratory

parameters in combination with early clinical outcome and radiological monitoring were examined. It can be stated that lean, REE-free bioabsorbable Mg screw fixation for medial malleolus fractures provided unimpeded fracture healing. All vital and laboratory parameters were normal and the patients presented very good functional outcomes.

In our opinion, resorbable implants such as Mg are the next step in a long history of orthopaedic implants. From this point of view, it is of utmost importance to clarify the way Mg implants work. Small radiolucency around the implants at early postoperative stages should not be misinterpreted as osteolysis. Despite this phenomenon, fracture healing was not adversely affected.

References

1. **Court-Brown CM**, **Caesar B**. Epidemiology of adult fractures: a review. *Injury*. 2006;37(8):691–697.
2. **Tile M**. Fractures of the Ankle. In: Schatzker J, Tile M, eds. *The Rationale of Operative Fracture Care*. 2nd ed. Berlin: Springer, 1996:523–561.
3. **Donatto KC**. Ankle fractures and syndesmosis injuries. *Orthop Clin North Am*. 2001;32(1):79–90.
4. **Shaffer MA**, **Okereke E**, **Esterhai JL**, **et al**. Effects of immobilization on plantar-flexion torque, fatigue resistance, and functional ability following an ankle fracture. *Phys Ther*. 2000;80(8):769–780.
5. **Keene DJ**, **Willett K**. Implications of the ankle injury management (AIM) trial: close contact casting or surgery for older adults with an unstable ankle fracture? *Bone Joint J*. 2019;101-B(12):1472–1475.
6. **Vandenborne K**, **Elliott MA**, **Walter GA**, **et al**. Longitudinal study of skeletal muscle adaptations during immobilization and rehabilitation. *Muscle Nerve*. 1998;21(8):1006–1012.
7. **Barnes H**, **Cannada LK**, **Watson JT**. A clinical evaluation of alternative fixation techniques for medial malleolus fractures. *Injury*. 2014;45(9):1365–1367.
8. **Femino JE**, **Gruber BF**, **Karunakar MA**. Safe zone for the placement of medial malleolar screws. *J Bone Joint Surg Am*. 2007;89(1):133–138.
9. **Buckley R**, **Kwek E**, **Duffy P**, **et al**. Single-Screw fixation compared with double screw fixation for treatment of medial Malleolar fractures: a prospective randomized trial. *J Orthop Trauma*. 2018;32(11):548–553.
10. **Keene DJ**, **Willett K**. Implications of the Ankle Injury Management (AIM) trial: close contact casting or surgery for older adults with an unstable ankle fracture? *Bone Joint J*. 2019;101-B(12):1472–1475.
11. **Walsh WR**, **Cotton NJ**, **Stephens P**, **et al**. Comparison of poly-L-lactide and polylactide carbonate interference screws in an ovine anterior cruciate ligament reconstruction model. *Arthroscopy*. 2007;23(7):757–765.
12. **Thormann U**, **Alt V**, **Heimann L**, **et al**. The biocompatibility of degradable magnesium interference screws: an experimental study with sheep. *Biomed Res Int*. 2015;2015:1–15.
13. **Wu L**, **Feyerabend F**, **Schilling AF**, **Willumeit-Römer R**, **Luthringer BJC**. Effects of extracellular magnesium extract on the proliferation and differentiation of human osteoblasts and osteoclasts in coculture. *Acta Biomater*. 2015;27:294–304.
14. **Jähn K**, **Saito H**, **Taipaleenmäki H**, **et al**. Intramedullary Mg2Ag nails augment callus formation during fracture healing in mice. *Acta Biomater*. 2016;36:350–360.
15. **Zhang Y**, **Xu J**, **Ruan YC**, **et al**. Implant-derived magnesium induces local neuronal production of CGRP to improve bone-fracture healing in rats. *Nat Med*. 2016;22(10):1160–.
16. **Pichler K**, **Kraus T**, **Martinelli E**, **et al**. Cellular reactions to biodegradable magnesium alloys on human growth plate chondrocytes and osteoblasts. *Int Orthop*. 2014;38(4):881–.
17. **Myrissa A**, **Bräuer S**, **Martinelli E**, **et al**. Gadolinium accumulation in organs of Sprague–Dawley® rats after implantation of a biodegradable magnesium-gadolinium alloy. *Acta Biomater*. 2017;48:521–529.
18. **Cheng M**, **Wahafu T**, **Jiang G-feng**, **et al**. A novel open-porous magnesium scaffold with controllable microstructures and properties for bone regeneration. *Sci Rep*. 2016;6:24134.
19. **Makkar P**, **Sarkar SK**, **Padalhin AR**, **et al**. In vitro and in vivo assessment of biomedical Mg–Ca alloys for bone implant applications. *J Appl Biomater Funct Mater*. 2018;16(3):126–136.
20. **Myrissa A**, **Agha NA**, **Lu Y**, **et al**. In vitro and in vivo comparison of binary Mg alloys and pure Mg. *Mater Sci Eng C*. 2016;61:865–874.
21. **Amerstorfer F**, **Fischerauer S**, **Fischer L**, **et al**. Long-term in vivo degradation behavior and near-implant distribution of resorbed elements for magnesium alloys WZ21 and ZX50. *Acta Biomater*. 2016;42:440–450.
22. **Jin L**, **Wu J**, **Yuan G**, **Chen T**. In vitro study of the inflammatory cells response to biodegradable Mg-based alloy extract. *PLoS One*. 2018;13(3):e0193276.
23. **Hofstetter J**, **Becker M**, **Martinelli E**, **et al**. High-strength low-alloy (HSLA) Mg–Zn–Ca alloys with excellent biodegradation performance. *JOM*. 2014;66(4):566–572.
24. **Grün NG**, **Holweg P**, **Tangl S**, **et al**. Comparison of a resorbable magnesium implant in small and large growing-animal models. *Acta Biomater*. 2018;78:378–386.
25. **Herscovici D**, **Scaduto JM**, **Infante A**. Conservative treatment of isolated fractures of the medial malleolus. *J Bone Joint Surg Br*. 2007;89-B(1):89–93.
26. **Kitaoka HB**, **Alexander IJ**, **Adelaar RS**, **et al**. Clinical rating systems for the ankle-hindfoot, midfoot, hallux, and lesser toes. *Foot Ankle Int*. 1994;15(7):349–353.
27. **Wichelhaus A**, **Emmerich J**, **Mittlmeier T**. A case of implant failure in partial wrist fusion applying Magnesium-Based headless bone screws. *Case Rep Orthop*. 2016;2016(2016):7049130.
28. **Meier G**, **Panzica R**. [First results with a resorbable MgYREZr compression screw in unstable scaphoid fractures show extensive bone cysts]. *Handchir Mikrochir Plast Chir*. 2017;49(1):37–41.
29. **Biber R**, **Pauser J**, **Geßlein M**, **Bail HJ**. Magnesium-Based absorbable metal screws for intra-articular fracture fixation. *Case Rep Orthop*. 2016;2016:9673174.
30. **Turan A**, **Kati YA**, **Acar B**, **Kose O**. Magnesium bioabsorbable screw fixation of radial styloid fractures: case report. *J Wrist Surg*. 2020;9(2):150–155.
31. **Plaass C**, **von Falck C**, **Ettinger S**, **et al**. Bioabsorbable magnesium versus standard titanium compression screws for fixation of distal metatarsal osteoto mies - 3 year results of a randomized clinical trial. *J Orthop Sci*. 2017;23(2):321–327.
32. **Windhagen H**, **Radtke K**, **Weizbauer A**, **et al**. Biodegradable magnesium-based screw clinically equivalent to titanium screw in hallux valgus surgery: short term results of the first prospective, randomized, controlled clinical pilot study. *Biomed Eng Online*. 2013;12:62.
33. **Plaass C**, **Ettinger S**, **Sonnow L**, **et al**. Early results using biodegradable magnesium screw for modified chevron osteotomies. *J Orthop Res*. 2016;34(12):2207–2214.
34. **Leonhardt H**, **Franke A**, **McLeod NMH**, **Lauer G**, **Nowak A**. Fixation of fractures of the condylar head of the mandible with a new magnesium-alloy biodegradable cannulated headless bone screw. *Br J Oral Maxillofac Surg*. 2017;55(6):623–625.
35. **Biber R**, **Pauser J**, **Brem M**, **Bail HJ**. Bioabsorbable metal screws in traumatology: A promising innovation. *Trauma Case Reports*. 2017;8:11–15.
36. **Kose O**, **Turan A**, **Unal M**, **Acar B**, **Guler F**. Fixation of medial malleolar fractures with magnesium bioabsorbable headless compression screws: short-term clinical and radiological outcomes in eleven patients. *Arch Orthop Trauma Surg*. 2018;138(8):1069–1075.
37. **Acar B**, **Kose O**, **Turan A**, **et al**. Comparison of bioabsorbable magnesium versus titanium screw fixation for modified distal chevron osteotomy in hallux valgus. *Biomed Res Int*. 2018;2018:1–9.
38. **Choo JT**, **Lai SHS**, **Tang CQY**, **Thevendran G**. Magnesium-based bioabsorbable screw fixation for hallux valgus surgery - A suitable alternative to metallic implants. *Foot Ankle Surg*. 2019;25(6):727–732.
39. **Klauser H**. Internal fixation of three-dimensional distal metatarsal I osteotomies in the treatment of hallux valgus deformities using biodegradable magnesium screws in comparison to titanium screws. *Foot Ankle Surg*. 2019;25(3):398–405.
40. **Gigante A**, **Setaro N**, **Rotini M**, **Finzi SS**, **Marinelli M**. Intercondylar eminence fracture treated by resorbable magnesium screws osteosynthesis: A case series. *Injury*. 2018;49(Suppl 3):S48–S53.
41. **Acar B**, **Unal M**, **Turan A**, **Kose O**. Isolated lateral Malleolar fracture treated with a bioabsorbable magnesium compression screw. *Cureus*. 2018;10(4):e2539.
42. **Aktan C**, **Ertan MB**, **Turan A**, **Kose O**. Fixation of small osteochondral fragments in a comminuted distal humerus fracture with magnesium bioabsorbable screws: a case report. *Cureus*. 2018;10(12):e3752.

Author information:
- P. Holweg
- V. Herber
- M. Ornig
- G. Hohenberger
- N. Donohue

■ P. Puchwein
■ A. Leithner
■ F. Seibert
Department of Orthopaedics and Trauma, Medical University of Graz, Graz, Austria.

Funding statement:
■ This study is supported by a LORENZ BÖHLER fond.

Contents lists available at ScienceDirect

Injury

journal homepage: www.elsevier.com/locate/injury

Screw placement in two different implants for proximal humeral fractures regarding regional differences in bone mineral density: An anatomical study

Patrick Holweg[a], Jan Dauwe[b,c,*], Peter Grechenig[a], Magdalena Holter[d], Mario Staresinic[e], Georg Feigl[f], Bore Bakota[a]

[a] Department of Orthopedics and Trauma Surgery, Medical University of Graz, Austria
[b] AO Research Institute, Davos, Switzerland
[c] Department of Orthopedics, University Hospitals Leuven, Belgium
[d] Institute for Medical Informatics, Statistics and Documentation, Medical University of Graz, Austria
[e] Department of Traumatology, Clinical Hospital Merkur, Zagreb, Croatia
[f] Institute of Anatomy, Medical University Graz, Austria

ARTICLE INFO

Article history:
Accepted 9 October 2020
Available online xxx

Keywords:
Proximal humerus plating
Drilling
Bone mineral density
Philos plate
Hofer plate

ABSTRACT

Background: The aim of this study was to investigate proximal humerus plating regarding drill depth and over penetration of the glenohumeral joint and to find a relation between these findings and different areas of bone mineral density (BMD) in the humeral head.

Material & Methods: The study sample involved 45 upper extremities from human adult cadavers. Two different plates (HOFER; PHILOS) were applied to the proximal humerus. Each hole was drilled until the respective participant thought to have placed the drill bit subchondral. Next, penetration of the far cortex was conducted to determine the residual bone stock. Additionally, the point of screw penetration of the far cortex was identified for each hole of the plates and allocated to five regions with different bone mineral density as described by Tingart et al.

Results: The screw penetration rate and the residual bone stock were compared within the 5 BMD regions. A significantly thicker residual bone stock was found at the central region (12.7 mm) than in the anterior region (9.5 mm) and in the posterior region (9.0 mm). The anterior region revealed a significantly higher penetration rate than the posterior region ($p = 0.01$) and the central region ($p = 0.03$).

Conclusion: The anterior region of the humeral head was associated with a higher over penetration rate of the far cortex into the glenohumeral joint and a decreased bone stock after subchondral drilling representing a reduced bone mineral density (BMD).

Level of evidence: Cadaver Study

Introduction

Proximal humerus fractures are common injuries in the elderly population and represent 4 to 5% of all fractures [1-3].

Regarding young patients, they are mostly the result of high-energy trauma, whereas in the elder population these fractures occur commonly due to osteoporotic bone constitution [4].

The treatment of proximal humerus fractures has been a very moving subject and is still a controversial topic in orthopaedic and trauma surgery. Currently, the literature lacks scientific evidence for the best treatment option. Although most of these fractures are stable and can be treated conservatively [5], a large variety of techniques has been described for their surgical treatment [6-9]. The surgical intervention is recommended for displaced fractures and commonly involves open reduction and internal plate fixation (ORIF). Unfortunately, clinically relevant complications following this procedure have been described by several authors [10-13]. In order to reduce the complication rate, anatomically pre-shaped plates, like the proximal humeral internal locking system (PHILOS, Synthes GmbH, Oberdorf, Switzerland) and the HOFER proximal

* Corresponding author: Jan Dauwe, MD, MSc, Catholic University Leuven, Belgium, 3000 Leuven.
E-mail address: dauwejan@gmail.com (J. Dauwe).

https://doi.org/10.1016/j.injury.2020.10.049
0020-1383/

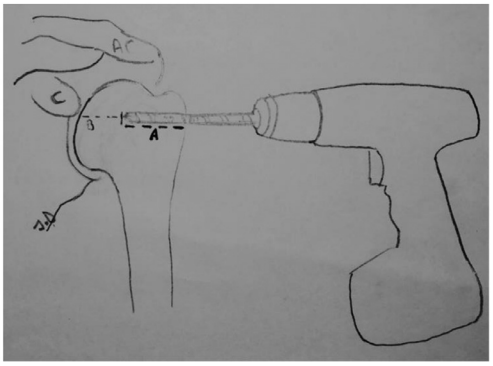

AC: acromion, C: coracoid process
A: distance drilled subchondral
B: residual bone stock (distance until point of cartilage perforation)

Fig. 1. Illustration of the subchondral drilling and the remaining bone stock.

humerus plate (Hofer GmbH, Fürstenfeld, Austria) were developed to improve screw fixation in the osteoporotic bone and to minimize soft tissue damage. Stable screw fixation is especially necessary in the osteoporotic bone, since osteoporotic fractures tend to be more complex with progress of the disease as postulated by Court-Brown et al. [14] These pre-shaped plates provide angular stability, which is especially useful in the osteoporotic bone [15-17] and recently published clinical studies show promising outcomes regarding their use [18,19]. Nevertheless, complication rates ranging up to 40%, including post-interventional dislocations as well as loss of reduction and screw cut-out have been reported [20].

The aim of this study was to investigate proximal humerus plating regarding over penetration of the glenohumeral joint and to find a correlation between the remaining bone stock after subchondral drilling (Fig. 1) and the different areas of bone mineral density (BMD) using a cadaver model. The different BMD areas in the humeral head were described by Tingart et al. [21]

Material and methods

The study sample involved 45 upper extremities from human adult cadavers embalmed using Thiel's solution [22,23]. The respective body donors gave their written informed consent to participate in anatomical studies during their lifetime. The collective consisted of 22 limbs from female and 23 upper extremities from male donors. Their age ranged from 57 to 93 years with a median of 74 years. Via inspection of the skin and soft tissues as well as through radiographic control with the C-arm, extremities with former fractures, surgical interventions or malformations in the region of interest had been excluded prior to the implementation of the study.

Plate application was performed by six orthopaedic surgeons (4 males, 2 females) with different levels of experience. In detail, the level of experience ranged from 6 months up to 38 years. All participants were aware of the study's purpose.

After complete dissection of the bones from the soft tissues, a PHILOS plate was applied according to the technical advices on the proximal humerus, one centimetre dorsal of the sulcus intertubercularis and one centimetre caudal of the tip of the greater tubercle (Fig. 2). After the drilling of all holes of the PHILOS plate, a HOFER proximal humerus plate was attached (Fig. 3). Since these two locking plates have different and not overlapping patterns of screw hole positioning, both could be used in succession on each humerus. To ensure a centred position of the screws in the hole with a fixed perpendicular angle, the Hofer aiming devise was

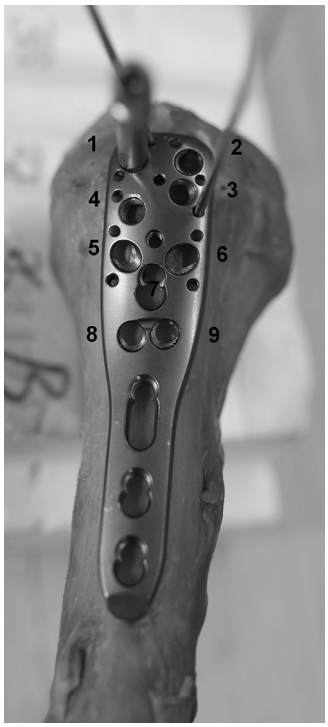

Fig. 2. Hole numbering in a PHILOS plate.

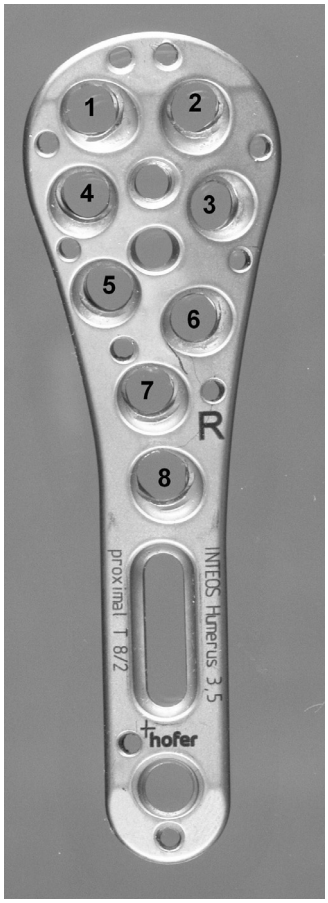

Fig. 3. Hole numbering in a HOFER plate.

Please cite this article as: P. Holweg, J. Dauwe, P. Grechenig et al., Screw placement in two different implants for proximal humeral fractures regarding regional differences in bone mineral density: An anatomical study, Injury, https://doi.org/10.1016/j.injury.2020.10.049

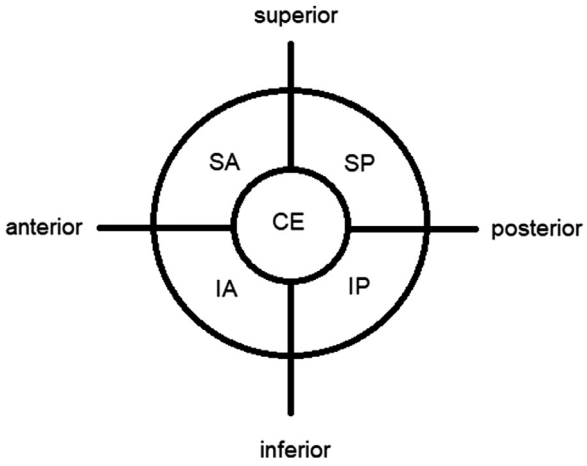

Fig. 4. Regions with different bone mineral density [superior-anterior (SA), inferior-anterior (IA), superior-posterior (SP), inferior-posterior (IP) and central (CE)] as described by Tingart et al.[21].

mounted before drilling. The possibility to drill the holes in variable angles in the Hofer plate was not used. The starting plate was changed every time. The plates were temporarily fixed to the bone with two 2-mm K-wires. As the next step a pre-shaped polystyrene plate was mounted to the bone's far cortex, the articular surface, to simulate the articular cavity. All drilling procedures were performed by use of a 2.7 mm drill bit with a Colibri II (Synthes GmbH, Oberdorf, Switzerland). Here, the participants were advised to drill perpendicular to the bone in accordance to the mounted drill guides as far as possible and to avoid overpenetration of the far cortex. The first hole was drilled until the respective participant thought to have placed the drill bit subchondral without intraoperative fluoroscopic surveillance. This value was then measured in millimetres using a depth gauge. Afterwards, penetration of the far cortex was conducted. This distance from entry to perforation was then used to determine the length of the residual bone stock after subchondral drilling (Fig. 1). Additionally, the point of screw penetration of the far cortex was examined for each hole of the plates and allocated to five regions with different bone mineral density [superior-anterior (SA), inferior-anterior (IA), superior-posterior (SP), inferior-posterior (IP) and central (CE)] as described by Tingart et al. [21](Fig. 4).

Statistical analysis

SAS software (version 9.4; SAS Institute, Inc., Cary, NC, USA) was used for the statistical analysis and a p-value <0.05 was considered significant. Categorical data are represented as frequencies and percentages; continuous variables are represented as mean, standard deviation (SD), median, minimum and maximum. The frequencies of possible iatrogenic screw penetrations were tested for significance with Fisher's exact test.

Results

In total, 46 PHILOS and 44 Hofer plates were tested. Regarding the unintended primary perforation rate of the far cortex, 11 holes (3.1%; total collective: 352 holes) were penetrated in the subgroup with the HOFER plate and in 22 holes (5,3%; total collective: 414 holes) the far cortex was perforated in the group using the PHILOS plate.

The specific penetration rates regarding the different drill holes of the plates are summarized in tables 1 and 2. In table 3 the average distance between the chosen point of the drill bit (subchondral) and the penetrated far cortex- the remaining bone stock- is shown for each hole of the two plates. In both plates the largest remaining bone stock was measured at hole 7 (Hofer: 11.2 mm; PHILOS 11.5 mm), whereas the shortest distance was found at hole 1 (Hofer: 6.4 mm) and hole 3 (PHILOS 6.3 mm).

Allocation of the screw holes to the appertaining regions described by Tingart et al. [21] revealed in the Hofer plate 2 screws in the superior-posterior (SP), 2 screws in the inferior-posterior (IP) and 2 screws in the central (CE) region. Only 1 screw was found in the anterior regions (SA/IA). Within the PHILOS group, 3 screws could be found in both superior regions (SA/SP). Each of the other 3 regions (IA/IP/CE) contained only 1 screw. (Table 4)

The correlation of bone drilling to the five regions described by Tingart et al. [21], revealed a significantly higher residual bone stock after drilling to the far cortex at the central region (12.7 mm) than in the anterior region (9.5 mm). Also the posterior region (9.0 mm) had less bone stock than the central region. There was no statistically significant difference in bone stock between the superior (8.3 mm) and inferior region (10.4 mm). Also no statistical difference was found between the posterior and the central region. The comparison of the two plates presented no significant differ-

Table 1
Penetration rates divided by holes in the subgroup: HOFER.

		n	percent
penetration	**hole 1**	2	18%
	hole 2	0	0%
	hole 3	3	27%
	hole 4	1	9%
	hole 5	0	0%
	hole 6	4	36%
	hole 7	1	9%
	hole 8	0	0%
total		11	100,0%

Table 2
Penetration rates divided by holes in the subgroup: PHILO.

		n	percent
penetration	**hole 1**	4	18%
	hole 2	3	14%
	hole 3	2	9%
	hole 4	3	14%
	hole 5	3	14%
	hole 6	1	5%
	hole 7	1	5%
	hole 8	4	18%
	hole 9	1	5%
total		22	100,0%

Table 3
Mean interval between the chosen point of the drill bit and the far cortex (remaining bone stock) in consideration of the different groups and holes.

Plate		n	mean	remaining bone stock	minimum	maximum
Hofer	S1	44	36.9	6.4	22.0	56.0
	S2	44	36.2	8.3	22.1	50.0
	S3	44	37.8	5.6	17.8	52.0
	S4	44	38.2	11.1	19.2	55.4
	S5	44	39.7	9.3	12.7	62.0
	S6	44	40.5	8	14.0	69.0
	S7	44	40.0	11.2	13.0	65.0
	S8	44	43.3	9.0	12.5	65.0
Philos	S1	46	41.2	7.8	29.0	53.0
	S2	46	41.3	9.2	21.0	51.0
	S3	46	45.5	6.3	29.2	60.0
	S4	46	42.5	8.0	26.0	58.2
	S5	46	43.6	7.4	29.0	56.0
	S6	46	42.8	11.2	27.0	59.0
	S7	46	45.4	11.5	21.6	60.0
	S8	46	48.7	8.3	19.0	60.0
	S9	46	46.0	8.8	15.0	61.0

Please cite this article as: P. Holweg, J. Dauwe, P. Grechenig et al., Screw placement in two different implants for proximal humeral fractures regarding regional differences in bone mineral density: An anatomical study, Injury, https://doi.org/10.1016/j.injury.2020.10.049

Table 4
Screw hole allocated to the regions defined by Tingart et al.[21].

		HOFER hole	PHILOS hole
regions	SA	3	1;3;5
	IA	6	8
	SP	1,2	2;4;6
	IP	4,5	9
	CE	7,8	7

ence regarding the remaining bone stock (Hofer: 11.36 mm; PHILOS: 8.62 mm).

The screw penetration rate was compared within the 5 regions. The anterior region revealed a significantly higher penetration rate than the posterior region ($p = 0.01$) and the central region ($p = 0.03$). The relation of the other regions showed no significant difference.

Discussion

The loosening of an implant and the screw perforation after internal plate fixation of displaced proximal humerus fractures are one of the techniques' major modes of osteosynthesis related failure. The screw length with a subchondral position in the humeral head is an important criterion for the stability of the osteosynthesis to avoid secondary dislocations [24–28].

In the present study, the areas in the humeral head with a higher bone mineral density were identified by measurement of the remaining bone stock after drilling to the far cortex (Fig. 1). These findings were correlated with the bone mineral density (BMD) described by Tingart et al. [21]

Tingart et al. [21] postulated a higher trabecular BMD at the CE than at SA and IA. The BMD at the superior level was lower than that at the inferior level. The posterior half of the humeral head showed a higher trabecular BMD than the anterior half. A significant correlation was found between the trabecular BMD and the pull-out strength of cancellous screws.

Also, Liew et al. [26] had similar conclusions with linear load-to-pull-out testing of cancellous screws in the humeral head. Highest fixation strength was achieved with screw placement in the centre of the humeral head. Frich et al. [29] examined the surface of the humeral head looking at the density and topographical strength of the subchondral bone using mechanical testing of bone cylinders from the human head. Maximum strength and stiffness were found at the most central and medial and anterior parts of the humeral head. Scola et al. [30] developed a torque measurement tool to determine local resistance to breakaway offered cancellous bone in the humeral head to quantify local bone quality. Posterior and proximal regions of the humeral head displayed better local bone property than the anterior regions. Screws aimed at the anterior region encountered statistically significantly lower bone quality than those aimed at the posterior region.

In this study, we found the highest residual bone stock at the central region (12.7 mm). The bone stock of the superior region (8.3 mm) was lower than in the inferior region (10.4 mm). The posterior (9.0 mm) and anterior region (9.5 mm) presented a similar bone stock remainder. Secondarily, we correlated the unintended over penetration by drilling within the 5 BMD regions. The anterior region revealed a significantly higher penetration rate than the posterior region ($p = 0.01$) and the central region ($p = 0.03$). The relation of the other regions showed no significant differences. These results match well with the findings of Tingart et al. [21] as we considered the thickness of the residual bone stock in direct correlation with the bone mineral density.

For maximal stability of the screws, a screw positioning as close as possible to the far cortex is recommended. Therefore, the different bone mineral densities should be considered by the surgeons. Besides the optimal distribution of the screws into the areas of high mineral bone density, the surgeon is advised to obtain a subchondral screw positioning by reflecting the higher mineral bone density in certain areas. Furthermore, surgeons should be very careful when placing screws in the superior- anterior region of the humeral head, because of the increased screw perforation risk we found in this area.

There has been some dispute about screw placement in consideration of plate systems in the humoral head. Therefore, we additionally compared the outcome of both plates in consideration of screw distribution. After drilling to the far cortex, an overall residual bone stock of 11.36 mm was found at the Hofer Plate, whereas the PHILOS plate revealed a bone stock of 8.62 mm. There was a statistically significant higher perforation rate in group with the PHILOS plate than in the Hofer group. We suggest the different distribution of the screws to be responsible for this result. The PHILOS system distributes 4 screws into the anterior region with lower BMD. Regarding the Hofer plate, only 2 screws were located in the anterior area.

Respecting the limitations of our study and based on the results of the current cadaveric study, we suggest that future plate designs should take the distribution and the direction of the screw holes into account which is particularly compromised in the peripheral zones of the humeral head. Screw placement in the inferior and central region should be aimed for.

Conclusion

The anterior region of the humeral head was associated with a higher over penetration rate of the far cortex into the glenohumeral joint. Areas of increased bone mineral density in the humeral head could be identified by evaluation of the remaining bone stock. The areas with a higher BMD value should be considered by surgeons for optimal screw placement.

Informed consent

Body donors gave their written informed consent during their lifetime.

Funding

This research did not receive any specific grant from funding agencies in the public, commercial, or not-for-profit sectors.

Disclosure

This paper is part of a supplement supported by The Croatian Trauma Society.

Declaration of Competing Interest

All authors declare that they have no conflict of interest.

References

[1] Court-Brown CM, Caesar B. Epidemiology of adult fractures: a review. Injury 2006;37:691–7. doi:10.1016/j.injury.2006.04.130.
[2] Kristiansen B, Barfod G, Bredesen J, Erin-Madsen J, Grum B, Horsnaes MW, Aalberg JR. Epidemiology of proximal humeral fractures. Acta Orthop Scand 1987;58:75–7.
[3] Lauritzen JB, Schwarz P, Lund B, McNair P, Transbøl I. Changing incidence and residual lifetime risk of common osteoporosis-related fractures. Osteoporos Int 1993;3:127–32.

Please cite this article as: P. Holweg, J. Dauwe, P. Grechenig et al., Screw placement in two different implants for proximal humeral fractures regarding regional differences in bone mineral density: An anatomical study, Injury, https://doi.org/10.1016/j.injury.2020.10.049

[4] Seeley DG, Browner WS, Nevitt MC, Genant HK, Scott JC, Cummings SR. Which fractures are associated with low appendicular bone mass in elderly women? The Study of Osteoporotic Fractures Research Group. Ann Intern Med 1991;115:837–42.
[5] Young TB, Wallace WA. Conservative treatment of fractures and fracture-dislocations of the upper end of the humerus. J Bone Joint Surg Br 1985;67:373–7.
[6] Ogiwara N, Aoki M, Okamura K, Fukushima S. Ender nailing for unstable surgical neck fractures of the humerus in elderly patients. Clin Orthop Relat Res 1996(330):173–80.
[7] Park MC, Murthi AM, Roth NS, Blaine TA, Levine WN, Bigliani LU. Two-part and three-part fractures of the proximal humerus treated with suture fixation. J Orthop Trauma 2003;17:319–25.
[8] Resch H, Povacz P, Fröhlich R, Wambacher M. Percutaneous fixation of three- and four-part fractures of the proximal humerus. J Bone Joint Surg Br 1997;79:295–300.
[9] Robinson CM, Page RS, Hill RM, Sanders DL, Court-Brown CM, Wakefield AE. Primary hemiarthroplasty for treatment of proximal humeral fractures. J Bone Joint Surg Am 2003;85-A:1215–23.
[10] Aggarwal S, Bali K, Dhillon MS, Kumar V, Mootha AK. Displaced proximal humeral fractures: an Indian experience with locking plates. J Orthop Surg Res 2010;5:60. doi:10.1186/1749-799X-5-60.
[11] Meier RA, Messmer P, Regazzoni P, Rothfischer W, Gross T. Unexpected high complication rate following internal fixation of unstable proximal humerus fractures with an angled blade plate. J Orthop Trauma 2006;20:253–60.
[12] Südkamp N, Bayer J, Hepp P, Voigt C, Oestern H, Kääb M, Luo C, Plecko M, Wendt K, Köstler W, Konrad G. Open reduction and internal fixation of proximal humeral fractures with use of the locking proximal humerus plate. Results of a prospective, multicenter, observational study. J Bone Joint Surg Am 2009;91:1320–8. doi:10.2106/JBJS.H.00006.
[13] Thalhammer G, Platzer P, Oberleitner G, Fialka C, Greitbauer M, Vécsei V. Angular stable fixation of proximal humeral fractures. J Trauma 2009;66:204–10. doi:10.1097/TA.0b013e31815ede7b.
[14] Court-Brown CM, Garg A, McQueen MM. The epidemiology of proximal humeral fractures. Acta Orthop Scand 2001;72:365–71. doi:10.1080/000164701753542023.
[15] Bandalović A, Cukelj F, Knežević J, Ostojić M, Pavić A, Parać Z, Rošin M. The Results of Internal Fixation of Proximal Humeral Osteoporotic Fractures with PHILOS Locking Plate. Psychiatr Danub 2014;26(Suppl 2):376–81.
[16] Björkenheim JM, Pajarinen J, Savolainen V. Internal fixation of proximal humeral fractures with a locking compression plate: a retrospective evaluation of 72 patients followed for a minimum of 1 year. Acta Orthop Scand 2004;75:741–5.
[17] Kim JJ, Kim JW, Yu HS, Lee HS, Oh HK. Factors affecting accurate drill sleeve insertion in locking compression plates. Orthop Traumatol Surg Res 2013;99:823–7. doi:10.1016/j.otsr.2013.04.013.
[18] Konrad G, Hirschmüller A, Audige L, Lambert S, Hertel R, Südkamp NP. Comparison of two different locking plates for two-, three- and four-part proximal humeral fractures–results of an international multicentre study. Int Orthop 2012;36:1051–8. doi:10.1007/s00264-011-1410-8.
[19] Kumar GN, Sharma G, Sharma V, Jain V, Farooque K, Morey V. Surgical treatment of proximal humerus fractures using PHILOS plate. Chin J Traumatol 2014;17:279–84.
[20] Faraj D, Kooistra BW, Vd Stappen WA, Werre AJ. Results of 131 consecutive operated patients with a displaced proximal humerus fracture: an analysis with more than two years follow-up. Eur J Orthop Surg Traumatol 2011;21:7–12. doi:10.1007/s00590-010-0655-z.
[21] Tingart MJ, Lehtinen J, Zurakowski D, Warner JJ, Apreleva M. Proximal humeral fractures: regional differences in bone mineral density of the humeral head affect the fixation strength of cancellous screws. J Shoulder Elbow Surg 2006;15:620–4. doi:10.1016/j.jse.2005.09.007.
[22] Thiel W. An arterial substance for subsequent injection during the preservation of the whole corpse. Ann Anat 1992;174:197–200.
[23] Thiel W. The preservation of the whole corpse with natural color. Ann Anat 1992;174:185–95.
[24] Instrum K, Fennell C, Shrive N, Damson E, Sonnabend D, Hollinshead R. Semitubular blade plate fixation in proximal humeral fractures: a biomechanical study in a cadaveric model. J Shoulder Elbow Surg 1998;7:462–6.
[25] Koval KJ, Blair B, Takei R, Kummer FJ, Zuckerman JD. Surgical neck fractures of the proximal humerus: a laboratory evaluation often fixation techniques. J Trauma 1996;40:778–83.
[26] Liew AS, Johnson JA, Patterson SD, King GJ, Chess DG. Effect of screw placement on fixation in the humeral head. J Shoulder Elbow Surg 2000;9:423–6. doi:10.1067/mse.2000.107089.
[27] Manner M, Rösch B, Roy K. Vascular injuries complicating osteosynthesis in proximal femur fractures. Unfallchirurg 1999;102:227–31.
[28] Williams GR Jr, Copley LA, Iannotti JP, Lisser SP. The influence of intramedullary fixation on figure-of-eight wiring for surgical neck fractures of the proximal humerus: a biomechanical comparison. J Shoulder Elbow Surg 1997;6:423–8.
[29] Frich LH, Jensen NC. Bone properties of the humeral head and resistance to screw cutout. Int J Shoulder Surg 2014;8:21–6. doi:10.4103/0973-6042.131851.
[30] Scola A, Gebhard F, Weckbach S, Dehner C, Schwyn R, Fliri L, Röderer G. Mechanical quantification of local bone quality in the humeral head: a feasibility study. Open Orthop J 2013;7:172–6. doi:10.2174/1874325001307010172.

Please cite this article as: P. Holweg, J. Dauwe, P. Grechenig et al., Screw placement in two different implants for proximal humeral fractures regarding regional differences in bone mineral density: An anatomical study, Injury, https://doi.org/10.1016/j.injury.2020.10.049